Atmos. Chem. Phys., 15, 5501–5519, 2015
www.atmos-chem-phys.net/15/5501/2015/
doi:10.5194/acp-15-5501-2015

Atmospheric Chemistry and Physics
Open Access

Impacts of emission reductions on aerosol radiative effects

J.-P. Pietikäinen[1], K. Kupiainen[2,3], Z. Klimont[2], R. Makkonen[4], H. Korhonen[1], R. Karinkanta[1], A.-P. Hyvärinen[1], N. Karvosenoja[3], A. Laaksonen[1], H. Lihavainen[1], and V.-M. Kerminen[4]

[1]Finnish Meteorological Institute, P.O. Box 503, 00101 Helsinki, Finland
[2]International Institute for Applied Systems Analysis, Schlossplatz 1, 2361 Laxenburg, Austria
[3]Finnish Environment Institute SYKE, P.O. Box 140, 00251 Helsinki, Finland
[4]Department of Physics, University of Helsinki, P.O. Box 44, 00014 Helsinki, Finland

Correspondence to: J.-P. Pietikäinen (joni-pekka.pietikainen@fmi.fi)

Received: 31 October 2014 – Published in Atmos. Chem. Phys. Discuss.: 17 December 2014
Revised: 9 April 2015 – Accepted: 2 May 2015 – Published: 20 May 2015

Abstract. The global aerosol–climate model ECHAM-HAMMOZ was used to investigate changes in the aerosol burden and aerosol radiative effects in the coming decades. Four different emissions scenarios were applied for 2030 (two of them applied also for 2020) and the results were compared against the reference year 2005. Two of the scenarios are based on current legislation reductions: one shows the maximum potential of reductions that can be achieved by technical measures, and the other is targeted to short-lived climate forcers (SLCFs). We have analyzed the results in terms of global means and additionally focused on eight subregions. Based on our results, aerosol burdens show an overall decreasing trend as they basically follow the changes in primary and precursor emissions. However, in some locations, such as India, the burdens could increase significantly. The declining emissions have an impact on the clear-sky direct aerosol effect (DRE), i.e. the cooling effect. The DRE could decrease globally 0.06–0.4 W m^{-2} by 2030 with some regional increases, for example, over India (up to 0.84 W m^{-2}). The global changes in the DRE depend on the scenario and are smallest in the targeted SLCF simulation. The aerosol indirect radiative effect could decline 0.25–0.82 W m^{-2} by 2030. This decrease takes place mostly over the oceans, whereas the DRE changes are greatest over the continents. Our results show that targeted emission reduction measures can be a much better choice for the climate than overall high reductions globally. Our simulations also suggest that more than half of the near-future forcing change is due to the radiative effects associated with aerosol–cloud interactions.

1 Introduction

The net radiative forcing caused by atmospheric aerosol particles originating from human activities is currently negative, thereby offsetting a major, yet poorly quantified, fraction of the global warming caused by anthropogenic greenhouse gas emissions (Boucher et al., 2013; Smith and Mizrahi, 2013). The lifetime of atmospheric aerosol particles is relatively short, which has two major implications. Firstly, the climatically important aerosol properties vary greatly in both space and time in the atmosphere (e.g. Kaufman et al., 2002). Secondly, and perhaps even more importantly, atmospheric aerosol concentrations respond rapidly to any changes in emissions of either primary aerosol particles or aerosol precursor gases.

Overall increases in aerosol emissions during the past decades have contributed to the so-called global dimming, i.e. the reduction of shortwave radiation reaching the surface, followed by some brightening due to later emission reductions in many regions of the world (e.g. Wild, 2009; Cermak et al., 2010; Haywood et al., 2011). In the near future, there is a pressure for further aerosol and aerosol precursor emission reductions due to the adverse health effects by atmospheric aerosol particles (e.g. Pope and Dockery, 2006; Rao et al., 2012). This has raised concerns about losing a significant fraction of the current aerosol cooling effect (Brasseur and Roeckner, 2005; Arneth et al., 2009; Raes and Seinfeld, 2009) and generated discussions on how to optimally realize future emission reductions (Löndahl et al., 2010; Shindell et al., 2012; Shoemaker et al., 2013; Smith and Mizrahi, 2013; Partanen et al., 2013).

The discussed mitigation strategies focus on reduction of black carbon (BC). While BC itself has an apparent warming effect in the present-day climate (e.g. Jacobson, 2010; Jones et al., 2011; Bond et al., 2013; Boucher et al., 2013), the usually co-emitted sulfur and organic compounds are effective cooling agents, substantially complicating the design of optimal emission reductions (Kopp and Mauzerall, 2010; Ramana et al., 2010; Wang et al., 2015). Furthermore, besides having a direct radiative effect (DRE) on solar radiation, particles containing BC can act as cloud condensation and ice nuclei (Prenni et al., 2009; Leaitch et al., 2010). The influence of BC emission changes on clouds and climate is potentially important yet poorly quantified (Chen et al., 2010a; Bahadur et al., 2012; Bond et al., 2013).

The relation between future aerosol emission changes, radiative forcing and climate has been investigated both globally (Kloster et al., 2008; Menon et al., 2008; Unger et al., 2009; Chen et al., 2010b; Bellouin et al., 2011; Makkonen et al., 2012; Gillett and Salzen, 2013; Levy et al., 2013; Smith and Bond, 2014; Wang et al., 2015) and over some continental regions (Mickley et al., 2012; Péré et al., 2012; Sillmann et al., 2013). While demonstrating potentially large regional effects, very few of these studies have simultaneously considered the following issues together: the direct and indirect aerosol effects, the role of different world regions' emissions in these effects and contrasting emission changes reflecting alternative emission control strategies. In this paper, we aim to bring new insight into these issues by investigating near-future changes in the aerosol direct and indirect radiative forcing globally as well as over a number of selected world regions as a result of emission changes according to four recently developed emission scenarios. The specific questions we are searching answers for are the following:

- how much is the aerosol radiative effect, or the radiative forcing by aerosols, expected to change during the next couple of decades compared with the present-day value?
- how do these changes differ over different world regions?
- what are the relative roles of direct and indirect effects?
- to what extent are these patterns influenced by targeted emission reductions?

The paper is structured as follows: first, the model and the emission modifications are described in Sect. 2; Sect. 3 presents a detailed analysis of the results and explains the emission reductions influences to the climate, followed by Sect. 4, in which the main conclusions are listed and further steps are discussed.

2 Methods

2.1 Model description

The main tool in this work is the global aerosol–climate model ECHAM-HAMMOZ (version ECHAM5.5-HAM2.0) (Zhang et al., 2012). This model version has the HAM aerosol module (Stier et al., 2005), which includes the M7 aerosol microphysical module by Vignati et al. (2004). ECHAM-HAMMOZ simulates all the major aerosol sources (both natural and anthropogenic), microphysical processes and sinks. It predicts the evolution of seven interacting internally and externally mixed aerosol modes in terms of their size distribution and composition. The simulated aerosol components are sulfate, BC, organic carbon (OC), sea salt and mineral dust. The aerosol module is coupled with the host model's large-scale cloud scheme (no influence on convective microphysics) and radiation module; thus, both the direct and indirect aerosol effects are simulated online (Lohmann and Hoose, 2009). The cloud droplet activation is calculated using a parametrization by Abdul-Razzak and Ghan (2000).

The aerosol characteristics simulated by ECHAM-HAMMOZ have been evaluated in several previous studies. For example, ECHAM-HAMMOZ was included in the AeroCom model intercomparison exercise analyzing the life cycles of dust, sea salt, sulfate, black carbon and particulate organic matter in 16 global aerosol models (e.g Huneeus et al., 2011; Mann et al., 2014; Tsigaridis et al., 2014). Furthermore, Zhang et al. (2012) evaluated the ECHAM5-HAM2 version, which is used in this study, against the AeroCom models and a large range of atmospheric measurements. These studies have shown that ECHAM-HAMMOZ can reproduce the main aerosol characteristics realistically. There are, however, still some deficiencies in the model, as was pointed out by the study from Zhang et al. (2012): "(i) positive biases in AOD over the ocean, (ii) negative biases in AOD and aerosol mass concentration in high-latitude regions and (iii) negative biases in particle number concentration, especially that of the Aitken mode, in the lower troposphere in heavily polluted regions". However, in this study, we do not concentrate on model evaluation as such (this has been already partly done in Henriksson et al., 2014), although we do compare our simulated aerosol burdens, lifetime and radiative effects to several previous model studies.

2.2 Emissions

In this work, new emission modules were implemented to ECHAM-HAMMOZ and some of the old ones were updated. In the following sections, the new and modified modules are described in more detail. The global emissions maps for BC, OC and sulfur dioxide (SO_2) based on the new emissions are shown in the Supplement (Figs. S1, S2 and S3). Note that volcanic, dimethyl sulfide, dust and sea salt emissions are left

Table 1. Yearly emissions fluxes for different sources, continental anthropogenic emission scenarios and aerosol species (GFED denotes the wildfire emissions): black carbon (BC), organic carbon (OC) and sulfuric dioxide (SO_2). The different geophysical areas are shown in Fig. 1. Note: the GFED emissions do not include agricultural waste burning sector because it is included in the GAINS emissions.

	Globe	Eu	India	W-China	E-China	Africa	E-USA	W-USA	S-America
BC emissions									
Refe2005 [Tg a^{-1}]	5.26	0.56	0.83	0.56	1.40	0.99	0.12	0.25	0.25
CLEC2020 [Tg a^{-1}]	5.12	0.35	0.99	0.64	1.32	1.14	0.09	0.15	0.24
CLEC2030 [Tg a^{-1}]	5.17	0.32	1.12	0.71	1.15	1.22	0.10	0.13	0.25
CLECC2020 [Tg a^{-1}]	4.96	0.35	0.94	0.61	1.26	1.09	0.10	0.17	0.24
CLECC2030 [Tg a^{-1}]	4.88	0.37	0.99	0.63	1.01	1.10	0.14	0.20	0.25
BCAdd2030 [Tg a^{-1}]	2.74	0.14	0.59	0.38	0.54	0.76	0.05	0.08	0.13
MTFR2030 [Tg a^{-1}]	2.55	0.11	0.54	0.36	0.53	0.76	0.04	0.05	0.09
Aviation 2005 [Gg a^{-1}]	0.53	0.12	0.01	0.01	0.04	0.03	0.06	0.13	0.02
Aviation 2020 [Gg a^{-1}]	0.96	0.21	0.02	0.01	0.07	0.05	0.11	0.23	0.04
Aviation 2030 [Gg a^{-1}]	1.24	0.27	0.03	0.02	0.09	0.07	0.14	0.29	0.05
Ships 2005 [Gg a^{-1}]	140.44	16.07	5.58	0.01	6.74	14.87	4.15	10.87	5.78
Ships 2020 [Gg a^{-1}]	161.37	18.46	6.41	0.02	7.75	17.08	4.77	12.49	6.65
Ships 2030 [Gg a^{-1}]	169.35	19.38	6.73	0.02	8.13	17.92	5.00	13.11	6.97
GFED 2005 [Gg a^{-1}]	181.74	0.01	0.06	0.07	0.46	168.57	0.11	0.20	3.91
OC emissions									
Refe2005 [Tg a^{-1}]	13.59	0.72	2.71	1.81	3.60	3.22	0.25	0.44	0.61
CLEC2020 [Tg a^{-1}]	13.56	0.56	2.89	1.90	3.04	3.85	0.23	0.34	0.63
CLEC2030 [Tg a^{-1}]	12.97	0.53	2.87	1.87	2.28	4.08	0.30	0.26	0.64
CLECC2020 [Tg a^{-1}]	13.01	0.57	2.72	1.79	2.85	3.66	0.22	0.37	0.63
CLECC2030 [Tg a^{-1}]	12.06	0.60	2.53	1.65	2.02	3.69	0.41	0.30	0.65
BCAdd2030 [Tg a^{-1}]	4.97	0.30	0.92	0.58	1.12	1.20	0.13	0.21	0.32
MTFR2030 [Tg a^{-1}]	2.44	0.14	0.50	0.30	0.55	0.71	0.05	0.07	0.09
Ships 2005 [Gg a^{-1}]	149.49	17.11	5.94	0.02	7.17	15.82	4.41	11.57	6.15
Ships 2020 [Gg a^{-1}]	171.33	19.60	6.81	0.02	8.23	18.13	5.06	13.26	7.06
Ships 2030 [Gg a^{-1}]	180.31	20.63	7.16	0.02	8.66	19.08	5.33	13.96	7.43
GFED 2005 [Gg a^{-1}]	1352.67	0.18	0.51	0.67	3.80	1247.37	1.09	1.64	31.12
SO_2 emissions									
Refe2005 [Tg a^{-1}]	92.79	11.93	6.97	4.85	33.01	7.81	4.70	12.06	2.63
CLEC2020 [Tg a^{-1}]	77.86	6.01	12.03	7.20	33.60	5.89	1.68	4.15	2.66
CLEC2030 [Tg a^{-1}]	79.88	6.24	17.48	9.89	29.36	5.86	1.38	3.70	3.00
CLECC2020 [Tg a^{-1}]	69.91	5.27	10.51	6.39	30.00	5.41	1.50	3.58	2.56
CLECC2030 [Tg a^{-1}]	55.64	4.62	10.90	6.08	19.50	4.49	0.94	2.61	2.51
BCAdd2030 [Tg a^{-1}]	77.84	6.18	17.00	9.63	28.49	5.69	1.37	3.65	2.94
MTFR2030 [Tg a^{-1}]	19.66	1.90	1.95	1.24	7.87	1.81	0.46	1.30	1.34
Ships 2005 [Tg a^{-1}]	13.00	1.49	0.52	0.00	0.62	1.38	0.38	1.01	0.54
Ships 2020 [Tg a^{-1}]	6.63	0.76	0.26	0.00	0.32	0.70	0.20	0.51	0.27
Ships 2030 [Tg a^{-1}]	6.30	0.72	0.25	0.00	0.30	0.67	0.19	0.49	0.26
GFED 2005 [Gg a^{-1}]	162.99	0.02	0.07	0.08	0.51	149.40	0.12	0.22	3.94

unmodified and follow the methods presented in Stier et al. (2005) and Zhang et al. (2012).

We analyzed the emissions and simulation results both globally and over eight different geographical regions. These regions, i.e. western United States (W-USA), eastern United States (E-USA), South America (S-America), Europe, Africa, India, western China (W-China) and eastern China (E-China), are shown in Fig. 1. The emission fluxes for different sources, scenarios and years are represented in Table 1.

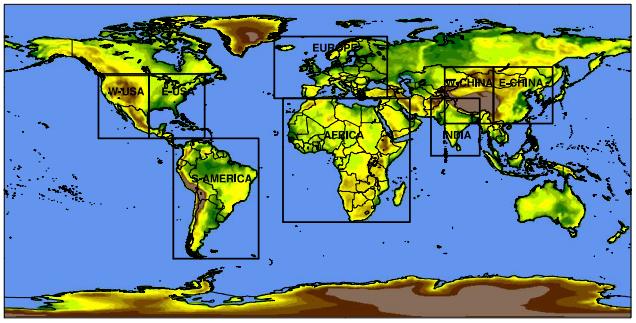

Figure 1. The separately analyzed areas: western United States (W-USA), eastern United States (E-USA), South America (S-America), Europe, Africa, India, western China (W-China) and eastern China (E-China).

2.2.1 Continental anthropogenic emissions

For continental anthropogenic emissions, we applied gridded data sets based on the GAINS (Greenhouse gas – Air pollution Interactions and Synergies) model (Amann et al., 2011), operated by the International Institute for Applied Systems Analysis (IIASA, http://gains.iiasa.ac.at). Globally, the GAINS model considers 162 geographical regions and includes all the major economic sectors. The principal statistical data used in the model for the base year (2005) in our simulations (simulation Refe2005) originate from the International Energy Agency (IEA) and The Statistical Office of the European Communities (EUROSTAT), whereas for agriculture the data are from United Nations Food and Agriculture Organization. We have used 2005 as a reference year as emissions in this year have been well evaluated and the emissions do not change significantly between 2005 and 2015 for BC and OC (Granier et al., 2011). Over the same time period, SO_2 emissions have been estimated to slightly decrease globally (10–15 %), although regionally, e.g. in India and China, the emissions may have increased (Klimont et al., 2013). For comparison of GAINS emissions against for example representative concentration pathways (RCP), see Granier et al. (2011).

In addition to the reference simulation, we considered four scenarios drawing on the energy projections presented in the World Energy Outlook 2009 (IEA, 2009) and including different assumptions of legislative and technological developments in the next few decades. The CLEC scenario includes all currently agreed air pollution policies and legislation and estimates impacts on emissions in 2020 and 2030 (simulations CLEC2020 and CLEC2030 respectively). The CLECC scenario includes these same policies but is further designed to keep the total forcing due to long-lived greenhouse gases at 450 ppm CO_2-equivalent level by the end of the century via CO_2 mitigation measures mostly targeting the energy and industrial sectors (simulations CLECC2020 and CLECC2030) – this scenario relies on the 2 °C (450 ppm) energy scenario developed by IEA (IEA, 2009). The main reductions in aerosol species between CLEC and CLECC occur in the residential, transport, energy and industry sectors and are the result of shifts away from the use fossil fuels as well as improvements in energy efficiency (IEA, 2009). In addition, two more scenarios for 2030 were used. The BCAdd scenario targets the short-lived climate forcers (SLCFs) by including a portfolio of most important measures that could yield the largest reductions in their global radiative forcing in 2030 (simulation BCadd2030). The details of such scenario have been described in UNEP (2011) and Shindell et al. (2012). In short, the principles behind the development of the BCAdd scenario are a selection of measures which result in net reduction of radiative forcing calculated using pollutant-specific Global Warming Potential values (UNEP, 2011). The measures reduce the emissions of not only BC but also OC, carbon monoxide (CO), non-methane volatile organic compounds and nitrogen oxides (NO_x), and the reduced amounts vary across the measures. Key air pollutant measures include advanced emission standards on diesel engines (including diesel particulate filters), clean cookstoves, pellet stoves and boilers, more efficient brick kilns and ban of agricultural burning. Thus, in terms of species used here, the reductions target BC and OC emissions. Measures with a relatively small net impact or increase in radiative forcing have been excluded from this portfolio. Lastly, the maximum technically feasible reduction (MTFR) scenario implements the maximum reduction potential of anthropogenic aerosol and SO_2 emissions with currently available technologies by the year 2030 (simulation MTFR2030). The MTFR scenario introduces the best available technology to a maximum extent while ignoring any potential economic and political barriers. In this scenario, no consideration is given to the direction of the change in aerosol radiative forcing, so measures that reduce strongly the emissions of SO_2, e.g. fuel gas desulfurization, are also included. The emission model used includes the end of pipe measures that remove pollutants from the exhaust. This means that it assumes that the use of most advanced particulate filters will reduce emissions of primary particular matter, selective catalytic reduction installations will bring NO_x emissions down from industrial boilers, etc. For more detailed description of the current legislation and the MTFR scenarios, see e.g. Cofala et al. (2007) and Klimont et al. (2009). More information about an overall emission scenario comparison can be found from Amann et al. (2013).

In this study, the detailed GAINS sectoral emissions were aggregated into six key categories: (1) agriculture (waste burning on fields), (2) residential and commercial combustion, (3) power plants, energy conversion, extraction, (4) industry (combustion and processing), (5) surface transportation and (6) waste. In addition, an extra sector for other SO_2 emissions not covered separately in GAINS was included (mainly industrial sources not included in the fourth category). Each of the sectors were allocated into a $0.5° \times 0.5°$

grid. The emissions from agriculture, residential and commercial combustion, surface transportation and waste sectors were emitted at the surface level. The energy sector emissions were released into the following model levels: 51.25 % to second lowest level, 45.3 % to third lowest level and 3.45 % to fourth lowest level. The industrial sector and the extra sector for SO_2 emissions had the same vertical emission height distribution: 95 % to surface and 5 % to second lowest level. The emission heights were based on Bieser et al. (2011).

By default, GAINS provides only the total annual emissions for all sectors. Considering the importance of temporal resolution for few key sectors, we developed monthly estimates for power plants and residential combustion. Specifically for the latter, we applied the method developed by Streets et al. (2003), who calculated the operating hours for stoves based on monthly mean temperature, i.e. $< 0\,^{\circ}\mathrm{C} \Rightarrow 16\,\mathrm{h\,d^{-1}}$, $0\text{–}5\,^{\circ}\mathrm{C} \Rightarrow 12\,\mathrm{h\,d^{-1}}$, $5\text{–}10\,^{\circ}\mathrm{C} \Rightarrow 6\,\mathrm{h\,d^{-1}}$ and $> 10\,^{\circ}\mathrm{C} \Rightarrow 3\,\mathrm{h\,d^{-1}}$. In our approach, the monthly mean temperatures were obtained from the Climatic Research Unit TS 3.1 data set (Harris et al., 2014) and the calculations were done in each grid box separately. Since our aim was to study the scenarios in current day climate conditions, the temperatures from 2005 were used also for the scenarios.

2.2.2 Aviation emissions

We implemented into ECHAM-HAMMOZ the monthly aviation emission produced in QUANTIFY (Quantifying the Climate Impact of Global and European Transport Systems) project (Lee et al., 2005; Owen et al., 2010). Concerning the aerosol species and precursors of interest in our work, only BC mass and number concentration are available (no data for OC or SO_2). The data are provided on a 1° resolution grid and on 23 levels using 610 m vertical steps. Since the QUANTIFY database provides emissions only for year 2000, we scaled the emission by 1.3355 in 2005, by 2.4 in 2020 and by 3.1 in 2030. These scaling factors were estimated based in Fig. 6 in Lee et al. (2010).

2.2.3 Wildfire emissions

The Global Fire Emissions Database (GFED) data set for the wildfire emissions was updated to version 3 (Giglio et al., 2010; van der Werf et al., 2010). The data have a 0.5° spatial resolution and are on a monthly time resolution. To make the emissions height dependent, the same approach as used by Dentener et al. (2006) with AeroCom emissions was applied. In this approach, based on location and type, the emissions are divided into six altitude regimes: 0–100, 100–500 m, 0.5–1, 1–2, 2–3 and 3–6 km. GFED 3 data set includes six different sectors: (1) deforestation and degradation fire emissions, (2) savanna fire emissions, (3) woodland fire emissions, (4) forest fire emissions, (5) agricultural waste burning and (6) tropical peatland burning (confined to Indonesia and Malaysian Borneo) (van der Werf et al., 2010). The fifth sector can be also found in the GAINS model output (see Sect. 2.2.1) and in this work the GAINS agriculture sector was used. Moreover, for all simulated years, the 2005 GFED emissions were used. The yearly emissions are represented in Table 1.

2.2.4 Shipping emissions

The international ship emissions used here were based on the improved ICOADS (International Comprehensive Ocean-Atmosphere Data Set) data by Wang et al. (2008). The ICOADS data set presents only a proxy grid on a 0.1° horizontal resolution, i.e. the data set gives the fraction of total global ship emissions that is emitted at each grid cell. The final gridded emissions were obtained by using the global proxy with the values from RCP 8.5 (Riahi et al., 2007) (for 2005, 2020 and 2030 separately). The sensitivity of the results to the chosen RCP was tested by repeating the reference simulation (Refe2005) using RCP 2.6 emissions. However, the difference between the two RCPs was found to be so small that no further analysis will be shown from RCP 2.6 simulations. Since the proxy does not include estimates on how the shipping routes will change in the future, the same emission pattern was used in all the simulations.

In the Arctic, we used an additional high-resolution emission inventory by Corbett et al. (2010). In this inventory, the data are given on a seasonal scale in a $5\,\mathrm{km} \times 5\,\mathrm{km}$ horizontal grid for 2004, including 2020 and 2030 as scenario years. We used the emission values for 2004 in our reference simulation for year 2005 without any modifications. It can be assumed that the error from this approach lies within the uncertainty limits of the emissions. For the scenario years 2020 and 2030, the business-as-usual approach was chosen. The scenarios also include changes in the shipping route patterns (details in Corbett et al., 2010). If there were overlapping grid boxes between ICOADS and Arctic emission data sets, the latter was chosen. The yearly shipping emissions are represented in Table 1.

2.3 Simulations

Each simulation was run for 5 years (2003–2007) preceded by a 6-month spin-up. In order to minimize the variation in the model meteorology, all the simulations were nudged, i.e. divergence, vorticity, surface pressure and temperature were nudged towards the ERA-Interim reanalysis data (Dee et al., 2011). The sea surface temperatures were taken from the Atmospheric Model Intercomparison Project (AMIP II) (Taylor et al., 2000). The 5-year monthly data were furthermore averaged to 1-year monthly data (multi-year monthly mean), which minimizes the influence of the internal variability of the model. All simulations were conducted at a T63 horizontal resolution (~ 200 km) with 31 vertical terrain following levels (top reaching 10 hPa).

Table 2. The global and regional mean burdens of black carbon (BC), organic aerosols (OA) and sulfate aerosols (SA) for the reference simulation and the difference of the mean burden between the scenarios and the reference simulation.

	Globe	Eu	India	W-China	E-China	Africa	E-USA	W-USA	S-America
BC burden									
Refe2005 [mg m^{-2}]	0.25	0.26	1.20	0.72	1.03	0.72	0.20	0.17	0.34
CLEC2020 Δ[%]	2.2	−27.5	17.0	14.6	−4.4	5.1	−22.8	−15.3	0.7
CLEC2030 Δ[%]	5.0	−30.3	31.9	28.4	−15.0	8.9	−23.1	−10.2	2.0
CLECC2020 Δ[%]	−0.2	−27.5	10.9	8.7	−9.0	2.9	−17.7	−13.5	0.2
CLECC2030 Δ[%]	0.9	−24.1	17.9	15.0	−24.6	4.7	−3.1	8.4	1.2
BCAdd2030 Δ[%]	−25.8	−63.5	−30.7	−33.2	−58.6	−13.5	−47.2	−40.5	−9.5
MTFR2030 Δ[%]	−27.1	−66.3	−35.8	−37.9	−58.2	−13.7	−54.5	−48.3	−12.6
OA burden									
Refe2005 [mg m^{-2}]	2.01	1.02	6.25	3.87	4.54	6.34	1.67	1.51	4.59
CLEC2020 Δ[%]	1.0	−6.3	5.3	4.8	−10.4	3.1	−3.1	−1.9	0.1
CLEC2030 Δ[%]	0.9	−7.4	6.1	5.5	−24.9	4.4	−3.8	4.3	0.5
CLECC2020 Δ[%]	−0.0	−6.1	0.4	0.2	−14.6	2.1	−2.0	−2.1	0.3
CLECC2030 Δ[%]	−1.1	−4.7	−3.7	−3.7	−30.7	2.3	−0.0	12.6	0.5
BCAdd2030 Δ[%]	−16.5	−25.1	−49.7	−47.1	−53.5	−11.9	−12.4	−13.2	−3.7
MTFR2030 Δ[%]	−21.0	−34.1	−63.1	−60.9	−64.8	−15.2	−18.8	−20.2	−5.3
SA burden									
Refe2005 [mg m^{-2}]	1.85	2.37	4.35	2.73	5.31	2.88	2.98	2.60	1.54
CLEC2020 Δ[%]	−8.7	−27.6	25.1	14.6	−1.1	−13.2	−38.8	−31.5	−4.9
CLEC2030 Δ[%]	−5.1	−26.0	62.2	42.1	−6.9	−9.5	−40.1	−32.9	−2.8
CLECC2020 Δ[%]	−12.3	−30.8	13.0	4.4	−10.2	−16.4	−42.1	−34.0	−5.9
CLECC2030 Δ[%]	−17.6	−35.1	11.8	0.8	−33.2	−20.8	−48.3	−40.8	−7.2
BCAdd2030 Δ[%]	−6.5	−27.2	57.5	37.4	−10.3	−10.9	−40.7	−33.5	−3.6
MTFR2030 Δ[%]	−36.7	−50.4	−59.5	−60.0	−66.3	−39.2	−58.5	−51.5	−15.9

We also made shorter simulations where the aerosol characteristics were compared to simulations with original emissions (not shown here). Based on these simulations, the new version reproduces closely the aerosol fields of the original model version.

3 Results and discussion

In the following we concentrate mainly on the 2030 simulation results and discuss briefly 2020 when it reveals additional information about the timescale of the emission reductions. All the absolute and relative changes presented are calculated as the difference between the scenario and reference simulation (Refe2005) values. In addition to global results, we analyze the simulations separately for the eight regions shown in Fig. 1. The column burdens and aerosol radiative effects for these regions are summarized in Tables 2 and 3.

3.1 Aerosol burdens

3.1.1 BC burden

The annual mean BC column burden is shown in Fig. 2. In all the simulations, the BC burden peaks in the Amazon region and central Africa (biomass burning areas), India (residential biomass burning area) and eastern China (industrial area). In these peak areas, changes in the BC burden are relatively modest in most of the scenarios apart from CLEC2030 which shows a 32 % increase over India, as well as BCAdd2030 and MTFR2030 which both show nearly 60 % decreases over eastern China (Table 2). Over India, the increase comes mainly from the traffic sector, which approximately doubles in CLEC2030. Even though the CLEC scenario includes current legislation measures, i.e. after some time new vehicles complying with existing standards will be in use, emissions start eventually to grow proportionally to the activity growth. However, it is noteworthy that the domestic sector will still have the biggest emissions over India. The decrease over eastern China in the two mitigation scenarios (BCAdd and MTFR) is primarily due to declining use of solid fuels (mostly coal) for cooking and heating in the residential combustion sector. The high BC burden areas in

Table 3. The global and regional mean clear-sky direct radiative effect (DRE) and cloud radiative effect (CRE) at the top of the atmosphere for the reference simulation and the changes in these (i.e. changes in aerosol radiative forcing) from the reference simulation to the future in different emission scenarios.

	Globe	Eu	India	W-China	E-China	Africa	E-USA	W-USA	S-America
DRE									
Refe2005 [W m^{-2}]	−3.94	−4.35	−4.16	−2.01	−5.16	−4.08	−3.97	−2.36	−3.59
CLEC2020 Δ[W m^{-2}]	0.13	0.56	−0.33	−0.04	0.07	0.16	0.90	0.51	0.05
CLEC2030 Δ[W m^{-2}]	0.11	0.54	−0.84	−0.20	0.29	0.15	0.95	0.54	0.03
CLECC2020 Δ[W m^{-2}]	0.16	0.61	−0.13	0.03	0.36	0.17	0.98	0.55	0.05
CLECC2030 Δ[W m^{-2}]	0.24	0.70	0.04	0.15	1.18	0.25	1.15	0.68	0.06
BCAdd2030 Δ[W m^{-2}]	0.06	0.51	−1.32	−0.60	0.12	−0.03	0.94	0.51	0.01
MTFR2030 Δ[W m^{-2}]	0.40	0.95	1.15	0.51	2.38	0.31	1.31	0.76	0.13
CRE									
Refe2005 [W m^{-2}]	−48.10	−51.05	−33.61	−37.14	−55.61	−31.55	−38.64	−33.87	−55.39
CLEC2020 Δ[W m^{-2}]	0.25	1.21	−0.10	−0.04	0.20	0.15	0.69	0.87	0.05
CLEC2030 Δ[W m^{-2}]	0.25	1.26	−0.16	−0.11	0.33	0.14	0.75	0.94	0.00
CLECC2020 Δ[W m^{-2}]	0.29	1.23	−0.02	0.07	0.26	0.17	0.76	0.89	0.03
CLECC2030 Δ[W m^{-2}]	0.38	1.42	−0.02	0.07	0.75	0.25	0.95	1.05	0.05
BCAdd2030 Δ[W m^{-2}]	0.38	1.59	0.18	0.24	1.07	0.40	0.78	1.02	0.18
MTFR2030 Δ[W m^{-2}]	0.82	2.51	0.98	0.98	2.77	0.70	1.47	1.72	0.55

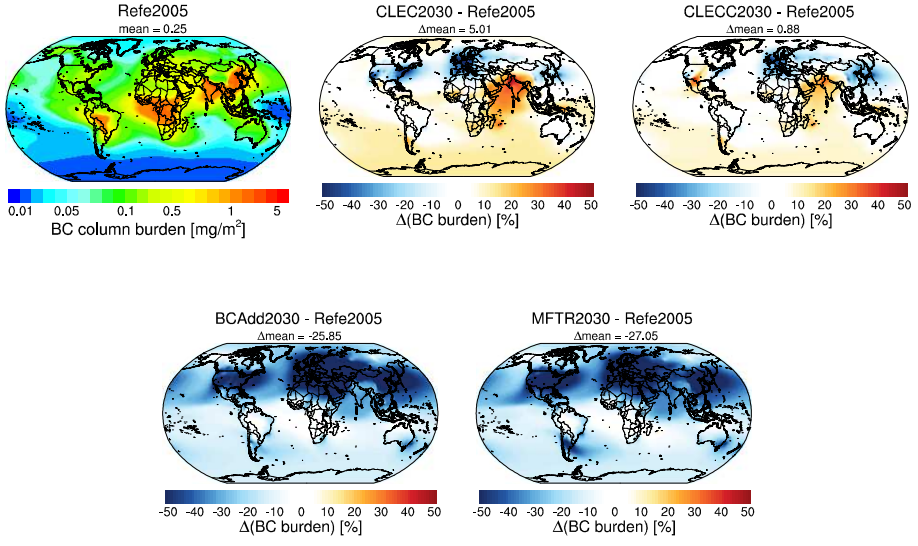

Figure 2. The annual mean black carbon (BC) burden in the reference run and the relative differences between the scenarios and the reference run.

the biomass burning regions of South America and Africa show negligible change in all the scenario runs because the GAINS scenarios do not predict reductions for this sector (and the wildfire emissions from GFED are the same for all simulated years).

In regions with lower absolute BC burden values, all the scenarios predict significant decreases by 2030 over Europe (−24 to −66 %, mainly from residential combustion and traffic sectors) and North America (−3 to −54 %, mainly traffic sector), although in CLECC2030 the burden slightly increases over Mexico and southern parts of USA (increment over western USA 8 %, caused by residential combustion sector). Furthermore, in the CLEC and CLECC scenarios, the BC burden increases over Africa (9 and 5 % respectively; from residential combustion sector) and western China (28 and 15 % respectively from residential combustion, traffic and industrial sectors). In these scenarios, small increases are seen also in southern Argentina, the west coast and southern parts of Africa and the border area of Indonesia and Papua New Guinea. There changes are caused by the overall emis-

sion increases over land areas in the Southern Hemisphere, as can be seen in Fig. S1. Partly due to atmospheric transport from continental areas and partly due to increased shipping emissions, the BC burden also increases over Antarctica as well as over most oceanic regions in the Southern Hemisphere. Although the absolute BC values in these regions are low, the increased burdens could lead to changes in the surface albedo over snowy and sea-ice-covered areas. In the CLEC2030 scenario, the burden also increases over the Arctic region. This is due to transport coming from southeastern Asia (around India), where the increased emissions cause increased values of BC at higher altitudes (lifting) which are eventually transported to the Arctic regions. In our analysis (details not shown here, but for more information please visit http://www.maceb.fi/result_viewer.html), we found that the lower-tropospheric BC burden decreases in CLEC and CLECC over the Arctic, but the transported BC from southeastern Asia makes the overall burden change quite small or even positive in the case of CLEC2030. A similar pathway for upper-tropospheric Arctic BC from southeastern Asia has been discussed already in a previous study by Stohl (2006). In any case, since the albedo change due to BC deposition is not included in the current model version, further investigation concerning BC effects on snowy regions is left for future studies.

The two other scenarios (BCAdd and MTFR) show a decreased BC burden over the whole globe (-26 and -27 % respectively). The differences between the burdens in these two scenarios are quite modest also on regional scales (Table 2), which means that the targeted sectors (transport and especially residential combustion) in BCAdd include most of the reduction potential of BC and very little further reductions can be obtained with additional technological measures (as in MTFR). These additional measures come from waste disposal and treatment as well as from agricultural waste burning. In the latter sector, the MTFR scenario assumes that all activity can be stopped and thus the emissions are set to 0.

Our reference simulation can be compared with previous model estimates on the atmospheric aerosol burden. Schulz et al. (2006) reported results from a multi-model comparison for global BC, organic aerosol (OA) and SO_4 burdens for the year 2000. In the subset of models using AeroCom emissions, the global ensemble mean for BC was $0.25\,\mathrm{mg\,m^{-2}}$ (standard deviation $\sigma = 0.08\,\mathrm{mg\,m^{-2}}$), whereas in the subset of model using other emission inventories, the global ensemble mean was $0.37\,\mathrm{mg\,m^{-2}}$ ($\sigma = 0.08\,\mathrm{mg\,m^{-2}}$). In addition, Bond et al. (2013) collected results from recent publications (some the same as in Schulz et al. (2006); details in the paper) and calculated a mean burden of $0.26\,\mathrm{mg\,m^{-2}}$. These results are in good agreement with our result of $0.25\,\mathrm{mg\,m^{-2}}$ (Table 2). Shindell et al. (2013) evaluated the Atmospheric Chemistry and Climate Model Intercomparison Project (ACCMIP) models and calculated the multi-model mean of BC burden in 2000 to be 0.16 Tg ($\sigma = 0.07$ Tg). Our equivalent value is 0.13 Tg for the year 2005. In a similar study (using older versions of both the ECHAM model and the IIASA emissions) Kloster et al. (2008) calculated the BC burden in 2000 to be 0.12 Tg. These results show that our updated emissions can reproduce similar global BC burdens. Kloster et al. (2008) also included two IIASA emission scenarios for 2030: a current legislation (CLE) scenario and a maximum feasible reduction (MFR) scenario. They reported burdens of 0.11 and 0.10 Tg respectively for the two scenarios. Our values are 0.13 Tg for CLEC2030 and CLECC2030 and 0.09 Tg for BCAdd and MTFR. The results do not differ much, so the different estimates are consistent with each other.

The residence time of aerosols is also one factor worth mentioning. In the reference simulation, we get a residence time of 6.0 days for BC. This compares well with earlier results, as shown by Textor et al. (2006), who did a multi-model comparison of the AeroCom models (simulating the year 2000). Authors reported that the BC residence time for ECHAM was 5.3 days while the mean for all the AeroCom models was 7.1 days ($\sigma = 33$ %). In addition, Shindell et al. (2013) reported the multi-model mean residence time of BC for 2000 to be 7.4 days ($\sigma = 3.4$ days), while Kloster et al. (2008) got 5.6 days in their year 2000 reference run, 5.8 days in 2030 CLE and 6.1 days in 2030 MFR. Our results indicate BC residence times of 6.3 days in CLEC2020 and CLECC2020, 6.4 days in CLEC2030 and CLECC2030, 6.6 days in BCAdd and 6.8 days in MTFR. The higher residence times in the scenarios reflect mainly the decreased washout due to less clouds, mainly caused by sulfate reductions (Lohmann and Feichter, 1997).

3.1.2 Organic aerosol burden

The absolute values of OA burden in the reference simulation (Fig. 3) are higher than those for the BC burden (almost by a factor of 10), but overall the burden maps are very similar. This reflects the fact that these two compounds are often co-emitted from the same sources, although organic emissions dominate in magnitude especially in the residential combustion sector. The OA burdens differ less between the different scenarios and show overall much smaller relative changes from the reference run than the BC burdens (Figs. 2 and 3). The main reason for this is that the current legislation measures do not have a major impact on domestic and agricultural sectors, which are two biggest sectors emitting OC (domestic is 5 times bigger than agricultural sector). This, together with unperturbed natural emissions, diminishes the differences seen in Fig. 3. However, the domestic sector will change quite dramatically (down to one-fifth of the reference) in the BCAdd and MTFR scenarios, which mainly explains the larger differences in the OA burden for these scenarios. Furthermore, the difference between BCAdd and MTFR can be explained by the agricultural sector, which, as was mentioned before, does not include any emissions in MTFR.

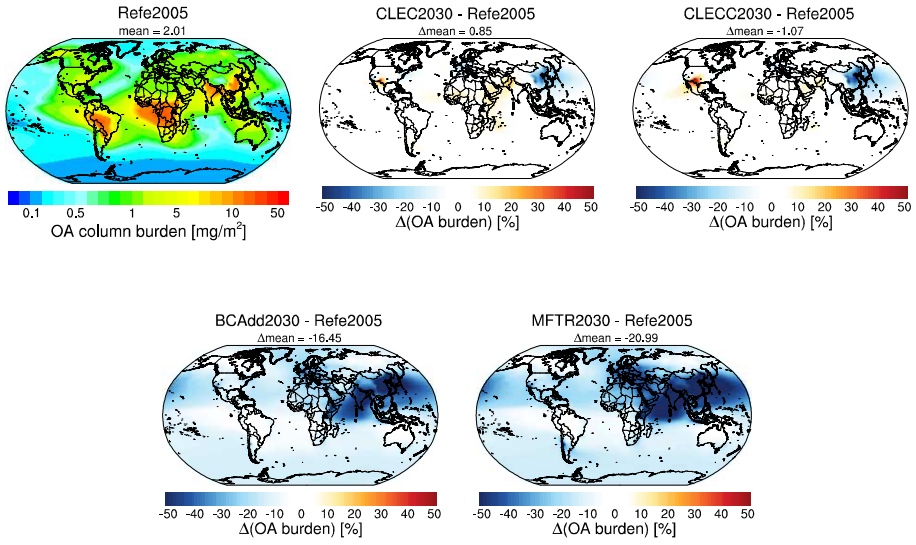

Figure 3. Like Fig. 2 but for organic aerosol (OA) burden.

The CLEC2030 and CLECC2030 scenarios predict the largest changes in the OA burden over eastern China (−25 and −31 % respectively) mainly from the residential combustion sector due to reduction of solid fuel use and effective decline of stove emissions. However, changes over India, Europe and North America are very small in contrast to the BC burden changes. The differing behaviour of BC and OA burdens can be explained by the traffic sector, in which BC emissions are impacted much more strongly than OC emissions. This is because the reductions in the traffic sector are targeted to diesel emissions, which is a high BC emitter.

In the BCAdd simulation, the OA burden decreases globally and the highest reductions are over Europe (−25 %, mainly from residential combustion and traffic sectors), India (−50 %, mainly residential combustion sector), western China (−47 %, residential combustion sector) and eastern China (−53 %, residential combustion and energy sectors). The geographical pattern of the change is similar in MTFR, although the decrement is higher; the highest reductions occur over China, Japan, India, Middle East and Europe reaching a −21 % decrement globally (all sectors decrease, with residential combustion sector having the biggest reductions). In these two scenarios, the pattern of the OA burden change is again quite different from the pattern of the BC burden change (Figs. 2 and 3). The OA burden change is much larger over India due to a very large contribution from both stoves and agricultural burning, and these two sources have a high share of OC. Larger BC changes are seen over Europe and North America as there are less stoves with high OC emissions, and instead most mitigation will be in diesel controls with a high BC share and some in the residential combustion sector. It is also noticeable that changes over the Southern Hemisphere are small in all the scenarios.

The values for the global OA burden from Schulz et al. (2006) are in good agreement with our results. Again, if only the models which used AeroCom-based emissions are taken into account, the global mean is 1.32 mg m^{-2} ($\sigma = 0.32$ mg m^{-2}). For the other models, Schulz et al. (2006) reported a mean of 2.40 mg m^{-2} ($\sigma = 0.39$ mg m^{-2}). Our results show a global OA burden of 2.01 mg m^{-2}, which falls into the range of the values reported in Schulz et al. (2006). Kloster et al. (2008) reported the OA burden to be 1.08 Tg in 2000, 1.00 Tg in 2030 CLE and 0.47 Tg in 2030 MFR. Our values for 2005 are 1.03 Tg and for 2030 they are 1.04 Tg in CLEC, 1.02 Tg in CLECC, 0.86 Tg in BCAdd and 0.81 in MTFR. Overall, the relatively large uncertainties in simulating the global and regional OA burdens arise from poorly quantified primary emissions and secondary organic aerosol formation, together with uncertainties in the sufficient complexity of the OA parametrizations (Tsigaridis et al., 2014).

The residence time of OA in our reference simulation was 5.8 days. Textor et al. (2006) reported for ECHAM a residence time of 5.4 days and overall AeroCom multi-model mean of 6.5 days ($\sigma = 27$ %), whereas Kloster et al. (2008) got 5.7 days. This means that, similar to BC, the residence times of OA in our simulations are in good accord with previous studies. Our future estimates show an OA residence time of 5.8 days in CLEC2020 and CLECC2020, 5.8 days in CLEC2030, 5.9 days in CLECC2030, 5.9 days in BCAdd and 6.0 days in MTFR. These are similar to Kloster et al. (2008) estimates: 5.8 days in CLE and 5.9 days in MFR.

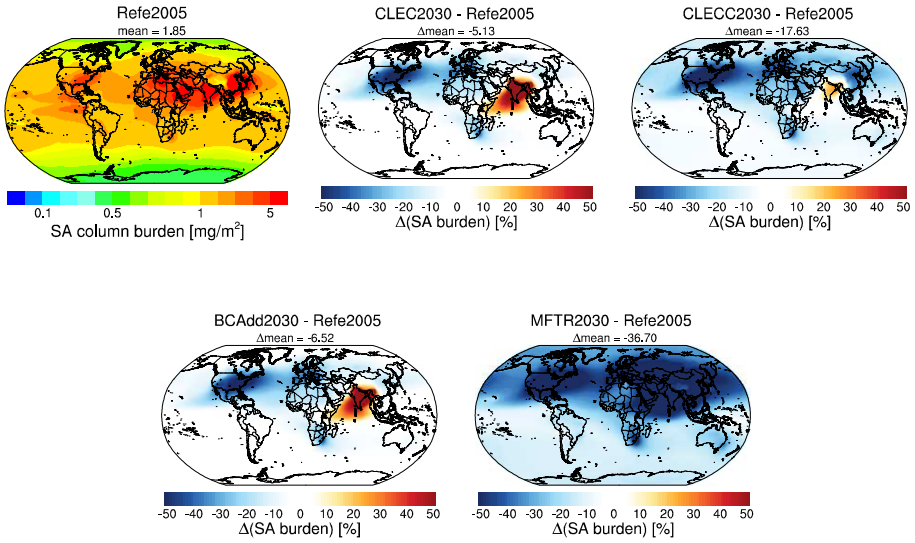

Figure 4. Like Fig. 2 but for sulfate aerosol (SA) burden.

3.1.3 Sulfate burden

The absolute sulfate aerosol (SA) burden map in Fig. 4 differs from the BC and OA maps, because the anthropogenic emission sources are more similar between BC and OC compared with SO_2. For BC and OC, the biggest source is the residential combustion sector, whereas SO_2 is mainly emitted from the industrial and energy sectors.

Figure 4 shows that the highest absolute values of the SA burden are over eastern China, India, Middle East, North Africa, southern Europe and eastern USA. The latitudinal dependence of the burden over the continents follows directly the emission pattern (Fig. S3).

In Europe, it is well known that sulfate precursor (SO_2) emissions have decreased over the last 2–3 decades (Hamed et al., 2010, and references therein). The same decreasing trend is also visible in the current legislation-based simulations, which have reductions from 26 % (CLEC2030) to 35 % (CLECC2030) over Europe. In North America, the reductions in the SA burden are even higher, especially over eastern and central parts of USA. CLEC2030 gives −33 % decrement over western USA and −40 % over eastern USA, whereas in CLECC2030 the values are −41 and −48 % respectively. These significant decreases in both Europe and North America are mainly from the energy sector, although the industrial sector has also reductions that influence the results.

Quite the opposite can be seen over India, where the SA burden will increase in all the scenarios, except in MTFR. The increment is smallest in the CLECC2030 scenario (12 %) and the highest in the CLEC2030 scenario (62 %), although almost as high an increase (58 %) is simulated in the BCAdd scenario. However, in the MTFR scenario the SA burden decreases by 60 %. These features come from the industrial and energy sectors and mean that the SA burden over India could be controlled with technical measures, such as flue gas desulfurization.

The global SA burden was also reported by Schulz et al. (2006). For model using AeroCom emissions, the global mean burden was 2.12 mg m^{-2} ($\sigma = 0.82$ mg m^{-2}) and for the other models 2.70 g m^{-2} ($\sigma = 1.09$ mg m^{-2}). The SA burden from our simulation is slightly lower at 1.85 mg m^{-2}. Shindell et al. (2013) got the multi-model mean of 2.0 Tg ($\sigma = 0.5$ Tg) for the SA burden. Our equivalent value is 0.95 Tg, which is more than 2 times lower. However, our result is close to the Kloster et al. (2008) estimate of 0.86 Tg. For the near future, Kloster et al. (2008) estimated that sulfate burden will be 0.94 Tg in CLE and 0.53 Tg in MFR. Our simulations show 0.90 Tg in CLEC2030, 0.78 Tg in CLECC2030, 0.88 Tg in BCAdd and 0.60 Tg in MTFR. Despite of all these differences, we feel confident in saying that our result shows a realistic global SA burden as there are differences in sources and sinks (e.g. different emission years, deposition modules etc).

For sulfate, the residence time in the reference simulation was 3.8 days. From Textor et al. (2006), ECHAM sulfate residence time was the same 3.8 days, while the AeroCom multimodel mean was 4.1 days ($\sigma = 18$ %). Shindell et al. (2013) reported that their multi-model mean for sulfate residence time was 5 days ($\sigma = 2$ days), whereas Kloster et al. (2008) got 4.4 days. Our results are comparable with all the previous studies. Our future estimates show a sulfate residence time of 3.9 days in CLEC2020 and CLECC2020, 4.0 days in CLEC2030, 4.1 days in CLECC2030, 4.0 days in BCAdd and 4.3 days in MTFR. These result are also in accord with Kloster et al. (2008), who simulated 4.6 days for CLE and 4.7 days for MFR.

3.1.4 Aerosol burdens in 2020

In order to explore the timeline of the emission reductions, we will shortly summarize the current legislation scenarios changes between 2005 and 2020. Details about the burden changes between these years are shown in Table 2 and Fig. S4.

Regarding the BC burden, the same general features which were visible in the CLEC2030 simulation can also be seen in CLEC2020. While the changes from 2005 through 2020 to 2030 do not follow a linear path, the CLEC2020 simulation shows overall the same global pattern as the CLEC2030 simulation (Fig. S4). Globally, the BC burden increases 2 % between 2005 and 2020 and 5 % between 2005 and 2030, indicating an accelerated BC emission rate in the 2020s mainly from the traffic sector. Regionally, the biggest contributors to the increased BC burden in the 2020s are India and western China (Table 2). In both of these regions, the relative BC burden change (from the reference year 2005) almost doubles between 2020 and 2030. However, there is a significant decrease in the BC burden in eastern China after 2020 (−4 % between 2005 and 2020, −15 % between 2005 and 2030). This is caused by the reductions in the residential combustion and energy sectors, although it should be mentioned that the traffic sector increases between 2020 and 2030 in eastern China roughly as much as energy sector decreases.

In the CLECC scenario, the global BC burden decreases slightly between 2005 and 2020 (−0.2 %) and increases between 2005 and 2030 (1 %). The reason for this is the same as in the CLEC scenario, i.e. the traffic sector. The geographical patterns of BC burden change are quite similar for the CLECC2020 and CLECC2030 scenarios, even though there are some significant differences over North America. At the border area of Mexico and USA, the BC burden change shows no clear signal by 2020, but there is an increase by 2030. This can be also seen from Table 2: over western USA the BC burden decreases 13 % by 2020 but increases 8 % by 2030. This feature comes from the residential combustion sector, which is estimated to increase quite significantly by 2030. The reason for this is that in CLECC the underlying idea is to move from fossil fuels to bio fuels and residential burning, which takes place mainly between 2020 and 2030. Another region with a large difference in CLECC between 2020 and 2030 is eastern China, where the BC burden change (with respect to 2005) will increase from −9 to −25 % and this comes from the reductions in residential combustion and energy sectors. Similarly as in CLEC, the reduction in the energy sector is roughly balanced out by the increased traffic sector.

The global OA burden changes are small in both scenarios. However, in the CLEC scenario, the burden increases 1.0 % between 2005 and 2020 and 0.9 % between 2005 and 2030, indicating a slight reduction during the 2020s. A much stronger reduction after 2020 takes place in the CLECC scenario as the OA burden change is −0.05 % by 2020 and −1 % by 2030. Regionally, the largest differences are over eastern China and the Mexico–USA border. The decrement over eastern China increases between 2020 and 2030 in CLEC from −10 to −25 % and in CLECC from −15 to −31 % and mainly comes from the residential combustion sector. Over the Mexico–USA border, the scenarios show no signal by 2020, but by 2030 both have a strong positive sign; over western USA the burden change in CLEC is −2 % by 2020 and 4 % by 2030 and in CLECC is −2 and 13 % respectively. As explained above, this is caused by the increases in residential combustion sector. In other regions the changes are quite small and do not show significant changes in the pattern of OA burden.

In terms of the global SA burden, most of the reductions already take place before 2020 in both scenarios and, in fact, the CLEC scenario predicts an increase of SA in the 2020s (change from year 2005 burden is −9 % by 2020 and −5 % by 2030). This increase in the SA burden takes place mainly because of the increment over India (from 25 % change in 2020 to 62 % change in 2030) and western China (from 15 to 42 %) and is caused by higher industrial and energy sector emissions. At the same time, Europe and both North and South America experience very low emission reductions, or even slight emission increases, in the 2020s. In the CLECC scenario, the decreasing global trend in the SA burden continues throughout the 2020s, although it slightly slows down: the change from 2005 burden is −12 % by 2020 and −18 % by 2030. This global decrease is mainly caused by the decreasing trend in emissions from the energy sector. In this scenario, all studied regions show decreasing SA burdens between 2020 and 2030, with the largest decrease taking place in eastern China (burden change of −10 % in 2020 and −33 % in 2030). Over the other regions, the reductions after 2020 are at most 6 percentage units.

3.2 Radiative effects

We will next investigate how the simulated changes in the aerosol burden translate into aerosol radiative effects. As the radiative effects presented in the following sections are mostly negative, i.e. they have a cooling effect, positive changes in radiative effects translate into a weaker cooling by aerosols and vice versa. This should be kept in mind when the radiative effect plots are analyzed. Additionally, the values given in the following sections refer to the top of the atmosphere and are obtained directly from the radiation scheme (parallel calls with and without aerosols/clouds).

3.2.1 Direct radiative effect

Aerosols scatter and absorb the incoming solar radiation and the sum of these is called the direct radiative effect. Investigating changes in the DRE between two time periods, or years, tells us how the direct radiative forcing by aerosols changes between these years in different emission scenarios.

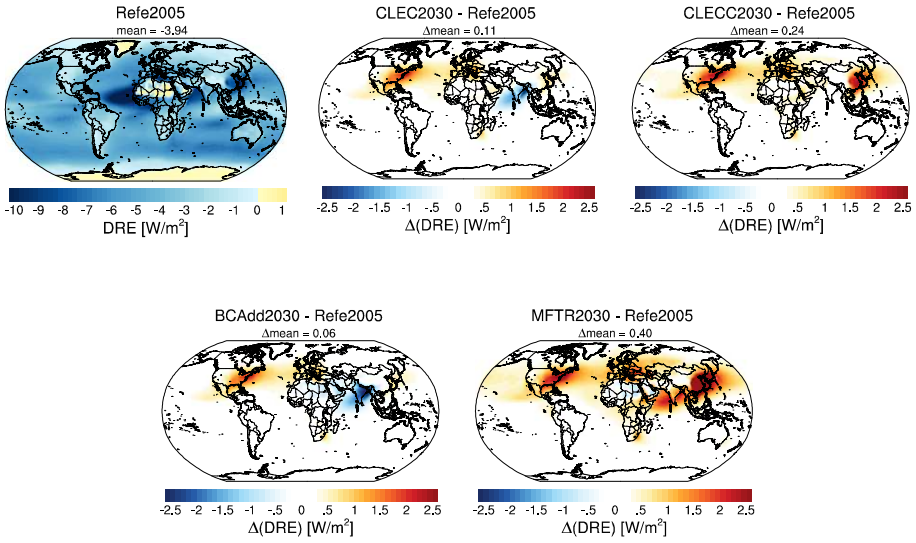

Figure 5. The yearly mean clear-sky direct radiative effect (DRE) at the top of the atmosphere in the reference run and the difference between scenarios and the reference run.

Besides short-wave radiation permutations, aerosols (especially large particles, for example dust) can also influence the long-wave radiation through absorption and emissivity. However, this is of minor importance for the small anthropogenic aerosols (Ramanathan and Feng, 2009). We have conducted tests to estimate the magnitude of the long-wave component in our simulations and, based on the results, the impact was found to be not important. Thus, the DRE in our analysis is only calculated for the short-wave radiation. It should also be noted that the DRE values are clear-sky values, which means that they are calculated assuming a zero cloud cover.

Figure 5 shows the annual mean DRE for the reference run and the difference plots for the scenarios. The reference run shows that overall, the DRE is negative around the world (global mean $-3.94\,\mathrm{W\,m^{-2}}$). Previous studies have shown similar estimates. For example, Yu et al. (2006) presented a review of DRE estimates and concluded it to be $-4.9 \pm 0.7\,\mathrm{W\,m^{-2}}$ over land and $-5.5 \pm 0.2\,\mathrm{W\,m^{-2}}$ over oceans. Since many of the satellite measurements only give estimates over oceans, we have also calculated the equivalent value and got $-4.68\,\mathrm{W\,m^{-2}}$ (globally). This can be compared with Zhao et al. (2008), who estimated an oceanic DRE of $-4.98 \pm 1.67\,\mathrm{W\,m^{-2}}$, and with Forster et al. (2007), who estimated from satellite remote sensing studies a value of $-5.4\,\mathrm{W\,m^{-2}}$ ($\sigma = 0.9\,\mathrm{W\,m^{-2}}$) over the oceans. Therefore, our simulations seem to give realistic values and are in good agreement with previous studies.

In the reference simulation, the strongest cooling effect caused by DRE takes place over the Atlantic ocean near the coast of eastern Africa; this is mainly because of the dust transport from Sahara. The overall aerosol burden is high over the polluted areas, including eastern China, where it leads to a DRE of $-5.16\,\mathrm{W\,m^{-2}}$. Over Europe, India, Africa and eastern USA, the values are quite close to the global mean, whereas in western China and western USA, they are only approximately half of it. Over limited regions, the DRE can also be positive (Fig. 5). This happens when the underlying surface has a high albedo and the aerosols above are absorbing. This occurs mainly over Sahara, Antarctica and Greenland. Seasonally, positive DRE could also be seen over the Arctic and other snow-covered regions. Note that DRE could be positive also if the absorbing aerosol are above clouds, but here we use only clear-sky values.

Consistent with reductions in aerosol emissions, all the scenario simulations predict a decreasing cooling effect by aerosols due to DRE over both Europe and North America. The decrease in the magnitude of the DRE is predicted to be 0.5–1.0 $\mathrm{W\,m^{-2}}$ over Europe, 0.9–1.3 $\mathrm{W\,m^{-2}}$ over eastern USA, and 0.5–0.8 $\mathrm{W\,m^{-2}}$ over western USA. The smallest changes are seen in the CLEC and CLECC scenarios and the largest in the MTFR scenario. These changes are mainly caused by reductions in SO_2 emissions, which lead to lower aerosol concentrations and thus decrease the cooling effect. The main sector causing these reductions is the energy production and distribution sector, which has the highest reductions in the CLECC and MTFR scenarios. These reductions are also visible over eastern China, where BCAdd and CLEC scenarios show modest reduction in the cooling effect due to DRE change (0.07 and 0.29 $\mathrm{W\,m^{-2}}$ respectively), whereas they are much higher in the CLECC and MTFR scenarios (1.18 and 2.38 $\mathrm{W\,m^{-2}}$ respectively).

The simulated changes over India show significant variation between the different scenarios. Our simulations predict that the cooling effect will increase in BCAdd and CLEC (-1.32 and $-0.84\,\mathrm{W\,m^{-2}}$ respectively), and no significant changes will occur in CLECC, whereas in MTFR the cool-

ing effect will decrease ($1.15\,W\,m^{-2}$). The reason for this behaviour can be drawn from the changes in aerosol component burdens (Figs. 2–4).

It was shown in Sect. 3.1.1 that over India the BC burden increases in the CLEC and CLECC scenarios and decreases in the BCAdd and MTFR scenarios. Since the DRE change does not follow this pattern, it is obvious that its sign does not directly follow the changes in the BC burden. The OA burden changes over India are fairly similar with the BC burden changes, but overall both changes are so small that they do not influence the DRE significantly. However, the SA burden increases in the BCAdd (58 %) and CLEC scenarios (62 %), has small changes in CLECC (12 %) and decreases in MTFR (−60 %). It is clear that apart from CLECC, the changes in the DRE follow quite systematically the changes in the SA burden. In the CLECC simulation, the increased absorption coming from the increased BC burden eliminates the cooling entirely (absorption maps are in the Supplement; Fig. S5). This means that, based on our model simulation predictions, the sign of DRE change over India is a combination of a warming component, for which the changes are mainly caused by the residential combustion sector, and a cooling component, for which the changes are mainly due to energy production and distribution sector. Naturally, the same counteracting effects from absorbing BC and scattering sulfate can occur in other locations but is particularly obvious over India in our simulations.

It is not straightforward to compare the simulated DRE changes to previously published estimates due to different baseline and scenario years and differences in emission scenarios between the studies. Unger et al. (2009) undertook sensitivity studies with NASA Goddard Institute for Space Studies (GISS) model for the future DRE change using 1995 as a reference year and 2050 as a scenario year. The authors reported a global net reduction of $0.179\,W\,m^{-2}$ between these years. Our CLEC simulation shows slightly lower reductions from 2005 to 2030 ($0.11\,W\,m^{-2}$) and a decreasing trend in the 2020s (change from 2005 to 2020 is $0.13\,W\,m^{-2}$). CLECC shows somewhat higher values ($0.24\,W\,m^{-2}$) than Unger et al. (2009) and no sign of a changing trend. The predicted DRE changes in BCAdd and MTFR are clearly lower and higher respectively than simulated in Unger et al. (2009). When comparing these two studies, it should be noted that some of the reductions assumed by Unger et al. (2009) may have taken place already before 2005, which we use as the reference year.

Szopa et al. (2013) simulated with a global Earth system model the present-day climate and future climate based on different RCP scenarios. Based on Fig. 14 in their work, we calculated the global and European forcing change between years 2005 and 2030. Globally, the change is 0.0–$0.125\,W\,m^{-2}$ (depending on the RCP scenario), whereas our simulations show a 0.06–$0.4\,W\,m^{-2}$ change (or 0.11–$0.24\,W\,m^{-2}$ if only CLEC and CLECC are considered). In Europe, Szopa et al. (2013) estimate a DRE change of 0.3–$0.7\,W\,m^{-2}$, whereas our simulations predict a 0.51–$0.95\,W\,m^{-2}$ change (0.54–$0.7\,W\,m^{-2}$ for CLEC and CLECC). Smith and Bond (2014) used the Global Change Assessment Model (GCAM) to estimate the future forcing change and calculated a global DRE change of $0.175\,W\,m^{-2}$ between 2005 and 2030. Overall, our estimates of DRE change are well in line with the previous studies, especially given that there are many differences between the models and simulation set-ups used.

Kloster et al. (2008) did not calculate absolute values of DRE, but they did calculate the forcing between 2000 and 2030 (equivalent to our Δ(DRE)). The authors showed that in their simulations Δ(DRE) is $-0.10\,W\,m^{-2}$ for CLE and $0.58\,W\,m^{-2}$ for MFR. Our results show a similar magnitude as CLE for the CLEC and CLECC scenarios but with opposite signs. This can be due to the different reference year, model version and overall emissions in the two studies. For MTFR, our prediction of $0.4\,W\,m^{-2}$ change is in a relatively good agreement with the Kloster et al. (2008) estimate for MFR.

Our simulations were limited to the coming few decades; however, there are earlier published estimates on how the aerosol effect will change by the end of the century. Chen et al. (2010b) reported a reduction of $0.12\,W\,m^{-2}$ between 2010 and 2100 based on three different models. Bellouin et al. (2011) showed that for the time period of 2000–2090, HadGEM2-ES model gives a $0.32\,W\,m^{-2}$ reduction without nitrate and $0.83\,W\,m^{-2}$ when nitrate is included. Based on Szopa et al. (2013), the change between 2005 and 2090 was estimated to be 0.15–$0.26\,W\,m^{-2}$, and based on Smith and Bond (2014) the change between 2005 and 2100 was estimated to be $0.47\,W\,m^{-2}$. These examples give some estimates on how DRE changes might continue after 2030.

3.2.2 Cloud radiative effect (CRE)

The cloud radiative effect is a sum of the short-wave and long-wave cloud radiative effects. Since the short-wave radiative effect is more dominant, the following analysis only includes the short-wave component and makes the CRE analysis more consistent with the DRE analysis. Therefore, as was with DRE, we only include the short-wave component when discuss the CRE.

The CRE was calculated based on the method proposed by Ghan (2013), which removes the effects of aerosol scattering and absorption. The double-moment cloud scheme used in this work takes into account cloud droplet activation (Sect. 2.1). Freshly emitted insoluble BC may act as ice nuclei and thus influence ice clouds directly. In case of warm clouds, only soluble aerosols have the potential to act as cloud condensation nuclei. BC is emitted as insoluble but can in our model become hygroscopic through condensation of sulfuric acid and coagulation with soluble particles.

Figure 6 shows the simulated global distribution of CRE and the difference plots between the reference year and sce-

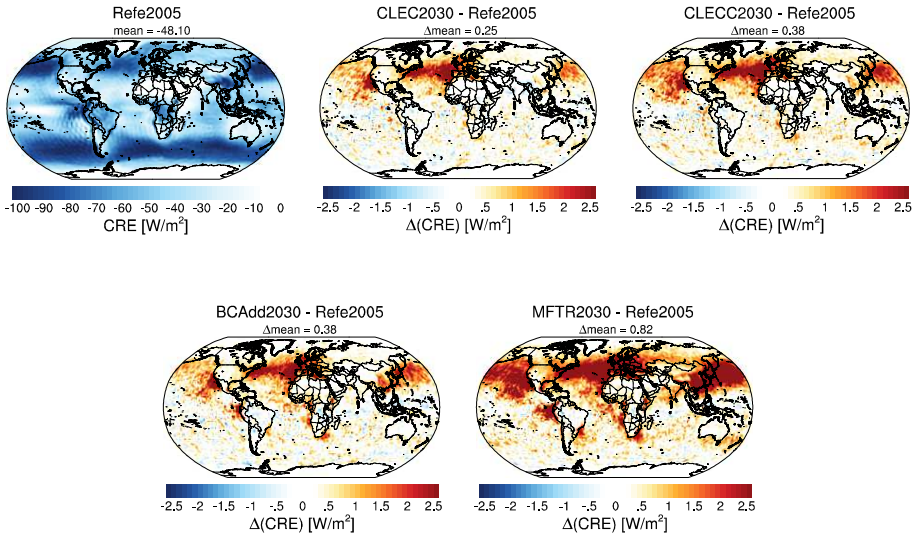

Figure 6. The yearly mean cloud radiative effect (CRE) at the top of the atmosphere in the reference run and the difference between scenarios and the reference run.

narios. The largest values of CRE are seen over oceans ($> 100\,\mathrm{W\,m^{-2}}$), mostly in temperate latitudes. Several continental areas, including Europe, China, central Africa, North America and South America, also have quite high CRE. All the scenario simulations show cooling due to future changes in the CRE. This takes place mainly in the Northern Hemisphere, where the change in CRE cooling effect is over $2.5\,\mathrm{W\,m^{-2}}$ in some areas. The reason for this is that most of the reductions in emissions are located in the Northern Hemisphere. In all the scenarios, the CRE cooling effect decreases over North Atlantic Ocean, North Pacific Ocean and Europe. Furthermore, BCAdd2030 and MTFR2030 show decreases also over eastern China and the coast of Peru. There are also other locations in MTFR2030 where decreases in CRE cooling effect can be seen, for example the east and west coasts of Africa and south coast of Brazil. Some minor changes also take place in MTFR over the Southern Hemisphere, but the values are very low ($< 0.5\,\mathrm{W\,m^{-2}}$). It is noteworthy that globally the absolute changes in CRE are approximately twice as large as the changes in the DRE (except for BCAdd, for which the CRE change is about 6 times as large as the DRE change). However, regionally large variability in the relative magnitudes of CRE and DRE changes can be seen.

The simulated patterns of CRE changes follow approximately the patterns of the BC and SA burden changes (Figs. 2 and 4). Over the Northern Pacific Ocean and west coast of South America, the BC burden change seems to be a more dominant contributor to the CRE change, whereas over Atlantic Ocean and coastal areas of Africa the SA burden changes are the dominant factor. Over India in the BCAdd scenario the increased SA burden does not lead to an increment in CRE values, because the influence is limited by reductions in BC.

Previously, Szopa et al. (2013) estimated the indirect forcing change to be 0.05–$0.1\,\mathrm{W\,m^{-2}}$ between 2005 and 2030. For the same time period, the estimate by Smith and Bond (2014) is $0.1\,\mathrm{W\,m^{-2}}$. These values are less than half of our simulated CRE change (0.25–$0.82\,\mathrm{W\,m^{-2}}$, Table 3). However, our model includes a sophisticated aerosol activation scheme that takes into account the aerosol number and composition size distribution and simulates both the first and second aerosol indirect effects. For example, Szopa et al. (2013) included only the first aerosol indirect effect and calculated the cloud droplet number concentration in a more simplistic way (based on soluble aerosol mass). Smith and Bond (2014) did not utilize a global atmospheric model at all but obtained their CRE estimates via direct scaling of aerosol emissions. Therefore, these two previous studies are not directly comparable to our simulations.

It should be stressed that the approach here only tells how the clouds react to aerosol concentration changes in current climate conditions as we used year 2005 meteorology in all simulations. Furthermore, some error is introduced by the nudging method because it restricts some of the feedback processes. For example, if emission reductions change the regional or global cloud features in a way that it should impact the overall circulation, these feedback processes will not be fully realized in our simulations. Nevertheless, our approach does show how clouds and their properties react to emission changes in current climatological conditions and gives indications on how the future cloud radiative effect might change.

3.2.3 Changes in aerosol radiative effect by the year 2020

We investigated the changes in radiative effects realized by year 2020 by looking into the current legislation simulation results (CLEC2020 and CLECC2020). The results are summarized in Table 3 and Fig. S6.

Our model results show that in CLEC, the reduction of global cooling due to DRE change takes place prior to 2020; the cooling effect even slightly increases between 2020 and 2030 (change from 2005 is $0.13\,W\,m^{-2}$ by 2020 and $0.11\,W\,m^{-2}$ by 2030). However, in CLECC the decrease in the global direct aerosol cooling effect continues after the 2020s; the DRE cooling effect change is $0.16\,W\,m^{-2}$ between 2005 and 2020 and $0.24\,W\,m^{-2}$ between 2005 and 2030. However, regional differences are large in both of the scenarios. For example, our model predicts that in the CLEC scenario the trend in the cooling effect will significantly accelerate between 2020 and 2030 over India and western China. For the same time period, the trend in the aerosol warming effect accelerates in eastern China. In the CLECC scenario, eastern and western China experience 3 and 5 times larger DRE change respectively from 2005 to 2030 than from 2005 to 2020. Over India, the negative change in DRE in 2020 (i.e. cooling effect with respect to 2005) turns into a positive change by 2030 (i.e. warming effect).

CRE changes after 2020 show somewhat different behaviour in the CLEC and CLECC scenarios. There is no further change in the global CRE in CLEC in the 2020s, whereas in CLECC the cooling effect due to CRE changes continues decreasing from $0.29\,W\,m^{-2}$ (between 2005 and 2020) to $0.39\,W\,m^{-2}$ (between 2005 and 2030). The global change in CLECC from 2020 to 2030 is mainly caused by the change over eastern China, where the CRE cooling effect changes from $0.26\,W\,m^{-2}$ by 2020 to $0.75\,W\,m^{-2}$ by 2030. This is caused by overall reductions in all aerosol species. Otherwise, the changes after 2020 are rather small in both of the scenarios, which means that most of the emission reduction based on CRE changes already takes place by 2020.

4 Summary and conclusions

We used the global aerosol–climate model ECHAM-HAMMOZ to evaluate how changes in the aerosol radiative effects, and hence forcing, are expected to decrease during the next couple of decades and how they are influenced by emission reductions. This was done by modifying the model to use new and updated emission modules. The most important update was the application of continental anthropogenic emissions produced by the GAINS model. With this version, four different emissions scenarios were investigated for the year 2030, and two of the scenarios where also run for the year 2020. Year 2005 was used as a reference year. The scenarios included two different current legislation scenarios (CLEC and CLECC), one targeted to short-lived climate forcers' emissions (BCAdd) and one introducing the maximum reduction potential of aerosols and SO_2 with currently available technologies (MTFR).

With the current legislation scenarios, the global BC aerosol burden was estimated to increase by 2030 compared with the current (2005) situation, the SA burden was estimated to decrease and the organic aerosol burden may change either way. In the same scenarios, the BC and OA burdens showed increase over India, western China, Africa and South America, and the SA burden showed increases over India and western China. The residential combustion and traffic sectors caused the majority of changes for BC and OC, while energy and industrial sectors caused most of the SA changes. Over South America, increases in the agricultural waste burning explained the higher burden for BC and OA in 2030. The targeted and maximum technological reductions showed decreasing trend for all species globally and regionally, except over India and western China. There, the BC targeted simulation increased SA burden due to emission increases in industrial and energy sectors.

The magnitude of negative aerosol radiative effect will decrease on a global scale in all the scenarios. Based on the current legislation scenarios, the cooling effect resulting from the clear-sky DRE, compared to the year 2005, will decrease by $0.11–0.24\,W\,m^{-2}$ by 2030. The technical maximum potential for DRE reductions is globally $0.4\,W\,m^{-2}$ by 2030. Regionally, the cooling effect from DRE changes can also increase, for example over India and western China. These changes follow mainly the BC and SA concentrations, which cause DRE changes of different signs. SA that has higher concentrations is more dominant and causes a cooling effect through scattering, while BC has the ability to absorb solar radiation and causes a heating effect. For example, over India the cooling effect from DRE was estimated to increase due to the increased SA burden, although in one of the current legislation simulations the warming effect coming from the increased BC burden cancelled out the cooling effect.

Our simulations suggest that the magnitude of the cloud radiative effect will decrease globally by $0.25–0.82\,W\,m^{-2}$ by 2030 compared with the year 2005. These changes and patterns are again connected to the BC and SA burden changes. Many of the changes occur already by 2020. Globally, the changes in the CRE cooling effect are roughly double the changes in DRE in most scenarios, but regionally large variability in the relative changes can be seen. For example, over India and western China the DRE change is larger than the CRE change. The changes in CRE take place over oceans, whereas the DRE changes are seen mostly over the continents. Regionally, India and western China are the only areas where the cooling effect from DRE and CRE is expected to increase. This is because of the aerosol burden increases over these two regions.

Our simulations predict a notable positive radiative forcing change in the current day climate conditions, up to about

$1\,W\,m^{-2}$ globally and $> 5\,W\,m^{-2}$ regionally, due to the reductions in aerosol and their precursor gas emissions that will take place during the next couple of decades. The magnitude of this forcing depends strongly on the chosen emission pathway. We have shown that targeted BC emission reductions are clearly the most beneficial for climate, making it even possible to achieve further enhancements in the negative direct radiative forcing (i.e. cooling effect) in some of the world regions (e.g. India and western China). To the contrary, reducing aerosol and their precursor emissions as much as it is technically feasible could be harmful for climate practically in all continental regions, although potentially beneficial from human health protection point of view. Finally, our simulations suggest that more than half of the near-future aerosol forcing change is due to the radiative effects associated with aerosol–cloud interactions. Noting this and the large uncertainties associated with this phenomenon (Boucher et al., 2013), more work is clearly needed for investigating the sources of cloud active aerosol particles into the atmosphere, aerosol–cloud–precipitation interactions and associated feedbacks in the climate system. Moreover, the use of coupled aerosol–chemistry models with more detailed aerosol description (e.g. including nitrates) would give more detailed estimates of the future forcing of aerosols.

The Supplement related to this article is available online at doi:10.5194/acp-15-5501-2015-supplement.

Acknowledgements. This work was supported by the EU Life+ project (LIFE09 ENV/FI/000572 MACEB), the Academy of Finland Research Programme for Climate Change FICCA (project 140748), an Academy research fellowship (decision 250348) and the EU FP7 IP PEGASOS (FP7-ENV-2010/265148). Gridding of the GAINS emission data by Chris Heyes is gratefully acknowledged. The ECHAM-HAMMOZ model is developed by a consortium composed of ETH Zurich, Max Planck Institut für Meteorologie, Forschungszentrum Jülich, University of Oxford and the Finnish Meteorological Institute and managed by the Center for Climate Systems Modeling (C2SM) at ETH Zurich.

Edited by: D. Spracklen

References

Abdul-Razzak, H. and Ghan, S. J.: A parameterization of aerosol activation: 2. Multiple aerosol types, J. Geophys. Res.-Atmos., 105, 6837–6844, doi:10.1029/1999JD901161, 2000.

Amann, M., Bertok, I., Borken-Kleefeld, J., Cofala, J., Heyes, C., Höglund-Isaksson, L., Klimont, Z., Nguyen, B., Posch, M., Rafaj, P., Sandler, R., Schöpp, W., Wagner, F., and Winiwarter, W.: Cost-effective control of air quality and greenhouse gases in Europe: Modeling and policy applications, Environ. Model. Softw., 26, 1489–1501, doi:10.1016/j.envsoft.2011.07.012, 2011.

Amann, M., Klimont, Z., and Wagner, F.: Regional and Global Emissions of Air Pollutants: Recent Trends and Future Scenarios, Annu. Rev. Environ. Res., 38, 31–55, doi:10.1146/annurev-environ-052912-173303, 2013.

Arneth, A., Unger, N., Kulmala, M., and Andreae, M. O.: Clean the Air, Heat the Planet?, Science, 326, 672–673, doi:10.1126/science.1181568, 2009.

Bahadur, R., Russell, L. M., Jacobson, M. Z., Prather, K., Nenes, A., Adams, P., and Seinfeld, J. H.: Importance of composition and hygroscopicity of BC particles to the effect of BC mitigation on cloud properties: Application to California conditions, J. Geophys. Res.-Atmos., 117, D09204, doi:10.1029/2011JD017265, 2012.

Bellouin, N., Rae, J., Jones, A., Johnson, C., Haywood, J., and Boucher, O.: Aerosol forcing in the Climate Model Intercomparison Project (CMIP5) simulations by HadGEM2-ES and the role of ammonium nitrate, J. Geophys. Res.-Atmos., 116, D20206, doi:10.1029/2011JD016074, 2011.

Bieser, J., Aulinger, A., Matthias, V., Quante, M., and van der Gon, H. D.: Vertical emission profiles for Europe based on plume rise calculations, Environ. Pollut., 159, 2935–2946, doi:10.1016/j.envpol.2011.04.030, 2011.

Bond, T. C., Doherty, S. J., Fahey, D. W., Forster, P. M., Berntsen, T., DeAngelo, B. J., Flanner, M. G., Ghan, S., Kärcher, B., Koch, D., Kinne, S., Kondo, Y., Quinn, P. K., Sarofim, M. C., Schultz, M. G., Schulz, M., Venkataraman, C., Zhang, H., Zhang, S., Bellouin, N., Guttikunda, S. K., Hopke, P. K., Jacobson, M. Z., Kaiser, J. W., Klimont, Z., Lohmann, U., Schwarz, J. P., Shindell, D., Storelvmo, T., Warren, S. G., and Zender, C. S.: Bounding the role of black carbon in the climate system: A scientific assessment, J. Geophys. Res.-Atmos., 118, 5380–5552, doi:10.1002/jgrd.50171, 2013.

Boucher, O., Randall, D., Artaxo, P., Bretherton, C., Feingold, G., Forster, P., Kerminen, V.-M., Kondo, Y., Liao, H., Lohmann, U., Rasch, P., Satheesh, S., Sherwood, S. B. S., and Zhang, X.: Clouds and Aerosols, in: Climate Change 2013: The Physical Science Basis. Contribution of Working Group I to the Fifth Assessment Report of the Intergovernmental Panel on Climate Change, edited by: Stocker, T. F., Qin, D., Plattner, G.-K., Tignor, M., Allen, S. K., Boschung, J., Nauels, A., Xia, Y., Bex, V., and Midgley, P. M., 571–658, Cambridge University Press, Cambridge, United Kingdom and New York, NY, USA, doi:10.1017/CBO9781107415324.016, 2013.

Brasseur, G. P. and Roeckner, E.: Impact of improved air quality on the future evolution of climate, Geophys. Res. Lett., 32, L23704, doi:10.1029/2005GL023902, 2005.

Cermak, J., Wild, M., Knutti, R., Mishchenko, M. I., and Heidinger, A. K.: Consistency of global satellite-derived aerosol and cloud data sets with recent brightening observations, Geophys. Res. Lett., 37, L21704, doi:10.1029/2010GL044632, 2010.

Chen, W.-T., Lee, Y. H., Adams, P. J., Nenes, A., and Seinfeld, J. H.: Will black carbon mitigation dampen aerosol indirect forcing?, Geophys. Res. Lett., 37, L09801, doi:10.1029/2010GL042886, 2010a.

Chen, W.-T., Nenes, A., Liao, H., Adams, P. J., Li, J.-L. F., and Seinfeld, J. H.: Global climate response to anthropogenic aerosol

indirect effects: Present day and year 2100, J. Geophys. Res.-Atmos., 115, D12207, doi:10.1029/2008JD011619, 2010b.

Cofala, J., Amann, M., Klimont, Z., Kupiainen, K., and Höglund-Isaksson, L.: Scenarios of global anthropogenic emissions of air pollutants and methane until 2030, Atmos. Environ., 41, 8486–8499, doi:10.1016/j.atmosenv.2007.07.010, 2007.

Corbett, J. J., Lack, D. A., Winebrake, J. J., Harder, S., Silberman, J. A., and Gold, M.: Arctic shipping emissions inventories and future scenarios, Atmos. Chem. Phys., 10, 9689–9704, doi:10.5194/acp-10-9689-2010, 2010.

Dee, D. P., Uppala, S. M., Simmons, A. J., Berrisford, P., Poli, P., Kobayashi, S., Andrae, U., Balmaseda, M. A., Balsamo, G., Bauer, P., Bechtold, P., Beljaars, A. C. M., van de Berg, L., Bidlot, J., Bormann, N., Delsol, C., Dragani, R., Fuentes, M., Geer, A. J., Haimberger, L., Healy, S. B., Hersbach, H., Hólm, E. V., Isaksen, L., Kållberg, P., Köhler, M., Matricardi, M., McNally, A. P., Monge-Sanz, B. M., Morcrette, J.-J., Park, B.-K., Peubey, C., de Rosnay, P., Tavolato, C., Thépaut, J.-N., and Vitart, F.: The ERA-Interim reanalysis: configuration and performance of the data assimilation system, Q. J. Roy. Meteor. Soc., 137, 553–597, doi:10.1002/qj.828, 2011.

Dentener, F., Kinne, S., Bond, T., Boucher, O., Cofala, J., Generoso, S., Ginoux, P., Gong, S., Hoelzemann, J. J., Ito, A., Marelli, L., Penner, J. E., Putaud, J.-P., Textor, C., Schulz, M., van der Werf, G. R., and Wilson, J.: Emissions of primary aerosol and precursor gases in the years 2000 and 1750 prescribed data-sets for AeroCom, Atmos. Chem. Phys., 6, 4321–4344, doi:10.5194/acp-6-4321-2006, 2006.

Forster, P., Ramaswamy, V., Artaxo, P., Berntsen, T., Betts, R., Fahey, D., Haywood, J., Lean, J., Lowe, D., Myhre, G., Nganga, J., Prinn, R., Raga, G., Schulz, M., and Dorland, R. V.: Changes in Atmospheric Constituents and in Radiative Forcing, in: Climate Change 2007: The Physical Science Basis, Contribution of Working Group I to the Fourth Assessment Report of the Intergovernmental Panel on Climate Change, edited by: Solomon, S., Qin, D., Manning, M., Chen, Z., Marquis, M., Averyt, K. B., Tignor, M., and Miller, H. L., Cambridge University Press, Cambridge, United Kingdom and New York, NY, USA, 2007.

Ghan, S. J.: Technical Note: Estimating aerosol effects on cloud radiative forcing, Atmos. Chem. Phys., 13, 9971–9974, doi:10.5194/acp-13-9971-2013, 2013.

Giglio, L., Randerson, J. T., van der Werf, G. R., Kasibhatla, P. S., Collatz, G. J., Morton, D. C., and DeFries, R. S.: Assessing variability and long-term trends in burned area by merging multiple satellite fire products, Biogeosciences, 7, 1171–1186, doi:10.5194/bg-7-1171-2010, 2010.

Gillett, N. P. and Salzen, K. V.: The role of reduced aerosol precursor emissions in driving near-term warming, Environ. Res. Lett., 8, 034008, doi:10.1088/1748-9326/8/3/034008, 2013.

Granier, C., Bessagnet, B., Bond, T., D'Angiola, A., Denier van der Gon, H., Frost, G. J., Heil, A., Kaiser, J. W., Kinne, S., Klimont, Z., Kloster, S., Lamarque, J.-F., Liousse, C., Masui, T., Meleux, F., Mieville, A., Ohara, T., Raut, J.-C., Riahi, K., Schultz, M. G., Smith, S. J., Thompson, A., van Aardenne, J., van der Werf, G. R., and van Vuuren, D. P.: Evolution of anthropogenic and biomass burning emissions of air pollutants at global and regional scales during the 1980–2010 period, Climatic Change, 109, 163–190, doi:10.1007/s10584-011-0154-1, 2011.

Hamed, A., Birmili, W., Joutsensaari, J., Mikkonen, S., Asmi, A., Wehner, B., Spindler, G., Jaatinen, A., Wiedensohler, A., Korhonen, H., Lehtinen, K. E. J., and Laaksonen, A.: Changes in the production rate of secondary aerosol particles in Central Europe in view of decreasing SO_2 emissions between 1996 and 2006, Atmos. Chem. Phys., 10, 1071–1091, doi:10.5194/acp-10-1071-2010, 2010.

Harris, I., Jones, P., Osborn, T., and Lister, D.: Updated high-resolution grids of monthly climatic observations – the CRU TS3.10 Dataset, Int. J. Climatol., 34, 623–642, doi:10.1002/joc.3711, 2014.

Haywood, J. M., Bellouin, N., Jones, A., Boucher, O., Wild, M., and Shine, K. P.: The roles of aerosol, water vapor and cloud in future global dimming/brightening, J. Geophys. Res.-Atmos., 116, D20203, doi:10.1029/2011JD016000, 2011.

Henriksson, S. V., Pietikäinen, J.-P., Hyvärinen, A.-P., Räisänen, P., Kupiainen, K., Tonttila, J., Hooda, R., Lihavainen, H., O'Donnell, D., Backman, L., Klimont, Z., and Laaksonen, A.: Spatial distributions and seasonal cycles of aerosol climate effects in India seen in a global climate-aerosol model, Atmos. Chem. Phys., 14, 10177–10192, doi:10.5194/acp-14-10177-2014, 2014.

Huneeus, N., Schulz, M., Balkanski, Y., Griesfeller, J., Prospero, J., Kinne, S., Bauer, S., Boucher, O., Chin, M., Dentener, F., Diehl, T., Easter, R., Fillmore, D., Ghan, S., Ginoux, P., Grini, A., Horowitz, L., Koch, D., Krol, M. C., Landing, W., Liu, X., Mahowald, N., Miller, R., Morcrette, J.-J., Myhre, G., Penner, J., Perlwitz, J., Stier, P., Takemura, T., and Zender, C. S.: Global dust model intercomparison in AeroCom phase I, Atmos. Chem. Phys., 11, 7781–7816, doi:10.5194/acp-11-7781-2011, 2011.

IEA: World Energy Outlook 2009, OECD Publishing, Paris, 650 pp. (612009191P1), ISBN: 9789264061309, 2009.

Jacobson, M. Z.: Short-term effects of controlling fossil-fuel soot, biofuel soot and gases, and methane on climate, Arctic ice, and air pollution health, J. Geophys. Res.-Atmos., 115, D14209, doi:10.1029/2009JD013795, 2010.

Jones, G. S., Christidis, N., and Stott, P. A.: Detecting the influence of fossil fuel and bio-fuel black carbon aerosols on near surface temperature changes, Atmos. Chem. Phys., 11, 799–816, doi:10.5194/acp-11-799-2011, 2011.

Kaufman, Y. J., Tanre, D., and Boucher, O.: A satellite view of aerosols in the climate system, Nature, 419, 215–223, 2002.

Klimont, Z., Cofala, J., Xing, J., Wei, W., Zhang, C., Wang, S., Kejun, J., Bhandari, P., Mathur, R., Purohit, P., Rafaj, P., Chambers, A., Amann, M., and Hao, J.: Projections of SO_2 , NO_x and carbonaceous aerosols emissions in Asia, Tellus B, 61, 602–617, doi:10.1111/j.1600-0889.2009.00428.x, 2009.

Klimont, Z., Smith, S. J., and Cofala, J.: The last decade of global anthropogenic sulfur dioxide: 2000–2011 emissions, Environ. Res. Lett., 8, 014003, doi:10.1088/1748-9326/8/1/014003, 2013.

Kloster, S., Dentener, F., Feichter, J., Raes, F., van Aardenne, J., Roeckner, E., Lohmann, U., Stier, P., and Swart, R.: Influence of future air pollution mitigation strategies on total aerosol radiative forcing, Atmos. Chem. Phys., 8, 6405–6437, doi:10.5194/acp-8-6405-2008, 2008.

Kopp, R. E. and Mauzerall, D. L.: Assessing the climatic benefits of black carbon mitigation, P. Natl. Acad. Sci. USA, 107, 11703–11708, doi:10.1073/pnas.0909605107, 2010.

Leaitch, W. R., Lohmann, U., Russell, L. M., Garrett, T., Shantz, N. C., Toom-Sauntry, D., Strapp, J. W., Hayden, K. L., Marshall, J., Wolde, M., Worsnop, D. R., and Jayne, J. T.: Cloud albedo increase from carbonaceous aerosol, Atmos. Chem. Phys., 10, 7669–7684, doi:10.5194/acp-10-7669-2010, 2010.

Lee, D., Pitari, G., Grewe, V., Gierens, K., Penner, J., Petzold, A., Prather, M., Schumann, U., Bais, A., Berntsen, T., Iachetti, D., Lim, L., and Sausen, R.: Transport impacts on atmosphere and climate: Aviation, Atmos. Environ., 44, 4678–4734, doi:10.1016/j.atmosenv.2009.06.005, 2010.

Lee, D. S., Owen, B., Graham, A., Fichter, C., Lim, L. L., and Dimitriu, D.: Allocation of International Aviation Emissions from Scheduled Air Traffic – Present Day and Historical (Report 2 of 3), Manchester Metropolitan University, Centre for Air Transport and the Environment, Manchester, UK, 2005.

Levy, H., Horowitz, L. W., Schwarzkopf, M. D., Ming, Y., Golaz, J.-C., Naik, V., and Ramaswamy, V.: The roles of aerosol direct and indirect effects in past and future climate change, J. Geophys. Res.-Atmos., 118, 4521–4532, doi:10.1002/jgrd.50192, 2013.

Lohmann, U. and Feichter, J.: Impact of sulfate aerosols on albedo and lifetime of clouds: A sensitivity study with the ECHAM4 GCM, J. Geophys. Res.-Atmos., 102, 13685–13700, doi:10.1029/97JD00631, 1997.

Lohmann, U. and Hoose, C.: Sensitivity studies of different aerosol indirect effects in mixed-phase clouds, Atmos. Chem. Phys., 9, 8917–8934, doi:10.5194/acp-9-8917-2009, 2009.

Löndahl, J., Swietlicki, E., Lindgren, E., and Loft, S.: Aerosol exposure versus aerosol cooling of climate: what is the optimal emission reduction strategy for human health?, Atmos. Chem. Phys., 10, 9441–9449, doi:10.5194/acp-10-9441-2010, 2010.

Makkonen, R., Asmi, A., Kerminen, V.-M., Boy, M., Arneth, A., Hari, P., and Kulmala, M.: Air pollution control and decreasing new particle formation lead to strong climate warming, Atmos. Chem. Phys., 12, 1515–1524, doi:10.5194/acp-12-1515-2012, 2012.

Mann, G. W., Carslaw, K. S., Reddington, C. L., Pringle, K. J., Schulz, M., Asmi, A., Spracklen, D. V., Ridley, D. A., Woodhouse, M. T., Lee, L. A., Zhang, K., Ghan, S. J., Easter, R. C., Liu, X., Stier, P., Lee, Y. H., Adams, P. J., Tost, H., Lelieveld, J., Bauer, S. E., Tsigaridis, K., van Noije, T. P. C., Strunk, A., Vignati, E., Bellouin, N., Dalvi, M., Johnson, C. E., Bergman, T., Kokkola, H., von Salzen, K., Yu, F., Luo, G., Petzold, A., Heintzenberg, J., Clarke, A., Ogren, J. A., Gras, J., Baltensperger, U., Kaminski, U., Jennings, S. G., O'Dowd, C. D., Harrison, R. M., Beddows, D. C. S., Kulmala, M., Viisanen, Y., Ulevicius, V., Mihalopoulos, N., Zdimal, V., Fiebig, M., Hansson, H.-C., Swietlicki, E., and Henzing, J. S.: Intercomparison and evaluation of global aerosol microphysical properties among AeroCom models of a range of complexity, Atmos. Chem. Phys., 14, 4679–4713, doi:10.5194/acp-14-4679-2014, 2014.

Menon, S., Unger, N., Koch, D., Francis, J., Garrett, T., Sednev, I., Shindell, D., and Streets, D.: Aerosol climate effects and air quality impacts from 1980 to 2030, Environ. Res. Lett., 3, 024004, doi:10.1088/1748-9326/3/2/024004, 2008.

Mickley, L., Leibensperger, E., Jacob, D., and Rind, D.: Regional warming from aerosol removal over the United States: Results from a transient 2010–2050 climate simulation, Atmos. Environ., 46, 545–553, doi:10.1016/j.atmosenv.2011.07.030, 2012.

Owen, B., Lee, D. S., and Lim, L.: Flying into the Future: Aviation Emissions Scenarios to 2050, Environ. Sci. Technol., 44, 2255–2260, doi:10.1021/es902530z, 2010.

Partanen, A. I., Laakso, A., Schmidt, A., Kokkola, H., Kuokkanen, T., Pietikäinen, J.-P., Kerminen, V.-M., Lehtinen, K. E. J., Laakso, L., and Korhonen, H.: Climate and air quality trade-offs in altering ship fuel sulfur content, Atmos. Chem. Phys., 13, 12059–12071, doi:10.5194/acp-13-12059-2013, 2013.

Péré, J., Colette, A., Dubuisson, P., Bessagnet, B., Mallet, M., and Pont, V.: Impacts of future air pollution mitigation strategies on the aerosol direct radiative forcing over Europe, Atmos. Environ., 62, 451–460, doi:10.1016/j.atmosenv.2012.08.046, 2012.

Pope, C. A. and Dockery, D. W.: Health effects of fine particulate air pollution: Lines that connect, J. Air Waste Manage., 56, 709–742, 2006.

Prenni, A. J., Petters, M. D., Kreidenweis, S. M., Heald, C. L., Martin, S. T., Artaxo, P., Garland, R. M., Wollny, A. G., and Pöschl, U.: Relative roles of biogenic emissions and Saharan dust as ice nuclei in the Amazon basin, Nat. Geosci., 2, 402–405, 2009.

Raes, F. and Seinfeld, J. H.: New directions: climate change and air pollution abatement: A bumpy road, Atmos. Environ., 43, 5132–5133, 2009.

Ramana, M. V., Ramanathan, V., Feng, Y., Yoon, S.-C., Kim, S.-W., Carmichael, G. R., and Schauer, J. J.: Warming influenced by the ratio of black carbon to sulphate and the black-carbon source, Nat. Geosci., 3, 542–545, 2010.

Ramanathan, V. and Feng, Y.: Air pollution, greenhouse gases and climate change: Global and regional perspectives, Atmos. Environ., 43, 37–50, doi:10.1016/j.atmosenv.2008.09.063, 2009.

Rao, S., Chirkov, V., Dentener, F., Van Dingenen, R., Pachauri, S., Purohit, P., Amann, M., Heyes, C., Kinney, P., Kolp, P., Klimont, Z., Riahi, K., and Schoepp, W.: Environmental Modeling and Methods for Estimation of the Global Health Impacts of Air Pollution, Environ. Model. Assess., 17, 613–622, doi:10.1007/s10666-012-9317-3, 2012.

Riahi, K., Gruebler, A., and Nakicenovic, N.: Scenarios of long-term socio-economic and environmental development under climate stabilization, Technol. Forecast. Soc., 74, 887–935, doi:10.1016/j.techfore.2006.05.026, 2007.

Schulz, M., Textor, C., Kinne, S., Balkanski, Y., Bauer, S., Berntsen, T., Berglen, T., Boucher, O., Dentener, F., Guibert, S., Isaksen, I. S. A., Iversen, T., Koch, D., Kirkevåg, A., Liu, X., Montanaro, V., Myhre, G., Penner, J. E., Pitari, G., Reddy, S., Seland, Ø., Stier, P., and Takemura, T.: Radiative forcing by aerosols as derived from the AeroCom present-day and pre-industrial simulations, Atmos. Chem. Phys., 6, 5225–5246, doi:10.5194/acp-6-5225-2006, 2006.

Shindell, D., Kuylenstierna, J. C. I., Vignati, E., van Dingenen, R., Amann, M., Klimont, Z., Anenberg, S. C., Muller, N., Janssens-Maenhout, G., Raes, F., Schwartz, J., Faluvegi, G., Pozzoli, L., Kupiainen, K., Höglund-Isaksson, L., Emberson, L., Streets, D., Ramanathan, V., Hicks, K., Oanh, N. T. K., Milly, G., Williams, M., Demkine, V., and Fowler, D.: Simultaneously Mitigating Near-Term Climate Change and Improving Human Health and Food Security, Science, 335, 183–189, doi:10.1126/science.1210026, 2012.

Shindell, D. T., Lamarque, J.-F., Schulz, M., Flanner, M., Jiao, C., Chin, M., Young, P. J., Lee, Y. H., Rotstayn, L., Mahowald, N., Milly, G., Faluvegi, G., Balkanski, Y., Collins, W. J., Conley,

A. J., Dalsoren, S., Easter, R., Ghan, S., Horowitz, L., Liu, X., Myhre, G., Nagashima, T., Naik, V., Rumbold, S. T., Skeie, R., Sudo, K., Szopa, S., Takemura, T., Voulgarakis, A., Yoon, J.-H., and Lo, F.: Radiative forcing in the ACCMIP historical and future climate simulations, Atmos. Chem. Phys., 13, 2939–2974, doi:10.5194/acp-13-2939-2013, 2013.

Shoemaker, J. K., Schrag, D. P., Molina, M. J., and Ramanathan, V.: What Role for Short-Lived Climate Pollutants in Mitigation Policy?, Science, 342, 1323–1324, doi:10.1126/science.1240162, 2013.

Sillmann, J., Pozzoli, L., Vignati, E., Kloster, S., and Feichter, J.: Aerosol effect on climate extremes in Europe under different future scenarios, Geophys. Res. Lett., 40, 2290–2295, doi:10.1002/grl.50459, 2013.

Smith, S. J. and Bond, T. C.: Two hundred fifty years of aerosols and climate: the end of the age of aerosols, Atmos. Chem. Phys., 14, 537–549, doi:10.5194/acp-14-537-2014, 2014.

Smith, S. J. and Mizrahi, A.: Near-term climate mitigation by short-lived forcers, P. Natl. Acad. Sci. USA, 110, 14202–14206, doi:10.1073/pnas.1308470110, 2013.

Stier, P., Feichter, J., Kinne, S., Kloster, S., Vignati, E., Wilson, J., Ganzeveld, L., Tegen, I., Werner, M., Balkanski, Y., Schulz, M., Boucher, O., Minikin, A., and Petzold, A.: The aerosol-climate model ECHAM5-HAM, Atmos. Chem. Phys., 5, 1125–1156, doi:10.5194/acp-5-1125-2005, 2005.

Stohl, A.: Characteristics of atmospheric transport into the Arctic troposphere, J. Geophys. Res.-Atmos., 111, D11306, doi:10.1029/2005JD006888, 2006.

Streets, D. G., Bond, T. C., Carmichael, G. R., Fernandes, S. D., Fu, Q., He, D., Klimont, Z., Nelson, S. M., Tsai, N. Y., Wang, M. Q., Woo, J.-H., and Yarber, K. F.: An inventory of gaseous and primary aerosol emissions in Asia in the year 2000, J. Geophys. Res.-Atmos., 108, 8809, doi:10.1029/2002JD003093, 2003.

Szopa, S., Balkanski, Y., Schulz, M., Bekki, S., Cugnet, D., Fortems-Cheiney, A., Turquety, S., Cozic, A., Déandreis, C., Hauglustaine, D., Idelkadi, A., Lathière, J., Lefevre, F., Marchand, M., Vuolo, R., Yan, N., and Dufresne, J.-L.: Aerosol and ozone changes as forcing for climate evolution between 1850 and 2100, Clim. Dynam., 40, 2223–2250, doi:10.1007/s00382-012-1408-y, 2013.

Taylor, K., Williamson, D., and Zwiers, F.: The sea surface temperature and sea-ice concentration boundary conditions for AMIP II simulations, Tech. Rep. PCMDI Report No. 60, Climate and Global Dynamics Division (CGD), Lawrence Livermore National Laboratory, Livermore, California, 2000.

Textor, C., Schulz, M., Guibert, S., Kinne, S., Balkanski, Y., Bauer, S., Berntsen, T., Berglen, T., Boucher, O., Chin, M., Dentener, F., Diehl, T., Easter, R., Feichter, H., Fillmore, D., Ghan, S., Ginoux, P., Gong, S., Grini, A., Hendricks, J., Horowitz, L., Huang, P., Isaksen, I., Iversen, I., Kloster, S., Koch, D., Kirkevåg, A., Kristjansson, J. E., Krol, M., Lauer, A., Lamarque, J. F., Liu, X., Montanaro, V., Myhre, G., Penner, J., Pitari, G., Reddy, S., Seland, Ø., Stier, P., Takemura, T., and Tie, X.: Analysis and quantification of the diversities of aerosol life cycles within AeroCom, Atmos. Chem. Phys., 6, 1777–1813, doi:10.5194/acp-6-1777-2006, 2006.

Tsigaridis, K., Daskalakis, N., Kanakidou, M., Adams, P. J., Artaxo, P., Bahadur, R., Balkanski, Y., Bauer, S. E., Bellouin, N., Benedetti, A., Bergman, T., Berntsen, T. K., Beukes, J. P., Bian, H., Carslaw, K. S., Chin, M., Curci, G., Diehl, T., Easter, R. C., Ghan, S. J., Gong, S. L., Hodzic, A., Hoyle, C. R., Iversen, T., Jathar, S., Jimenez, J. L., Kaiser, J. W., Kirkevåg, A., Koch, D., Kokkola, H., Lee, Y. H, Lin, G., Liu, X., Luo, G., Ma, X., Mann, G. W., Mihalopoulos, N., Morcrette, J.-J., Müller, J.-F., Myhre, G., Myriokefalitakis, S., Ng, N. L., O'Donnell, D., Penner, J. E., Pozzoli, L., Pringle, K. J., Russell, L. M., Schulz, M., Sciare, J., Seland, Ø., Shindell, D. T., Sillman, S., Skeie, R. B., Spracklen, D., Stavrakou, T., Steenrod, S. D., Takemura, T., Tiitta, P., Tilmes, S., Tost, H., van Noije, T., van Zyl, P. G., von Salzen, K., Yu, F., Wang, Z., Wang, Z., Zaveri, R. A., Zhang, H., Zhang, K., Zhang, Q., and Zhang, X.: The AeroCom evaluation and intercomparison of organic aerosol in global models, Atmos. Chem. Phys., 14, 10845–10895, doi:10.5194/acp-14-10845-2014, 2014.

UNEP: Near-term Climate Protection and Clean Air Benefits: Actions for Controlling Short-Lived Climate Forcers, united Nations Environment Programme (UNEP), Nairobi, Kenya, 78 pp., 2011.

Unger, N., Menon, S., Koch, D. M., and Shindell, D. T.: Impacts of aerosol-cloud interactions on past and future changes in tropospheric composition, Atmos. Chem. Phys., 9, 4115–4129, doi:10.5194/acp-9-4115-2009, 2009.

van der Werf, G. R., Randerson, J. T., Giglio, L., Collatz, G. J., Mu, M., Kasibhatla, P. S., Morton, D. C., DeFries, R. S., Jin, Y., and van Leeuwen, T. T.: Global fire emissions and the contribution of deforestation, savanna, forest, agricultural, and peat fires (1997–2009), Atmos. Chem. Phys., 10, 11707–11735, doi:10.5194/acp-10-11707-2010, 2010.

Vignati, E., Wilson, J., and Stier, P.: M7: An efficient size-resolved aerosol microphysics module for large-scale aerosol transport models, J. Geophys. Res.-Atmos., 109, D22202, doi:10.1029/2003JD004485, 2004.

Wang, C., Corbett, J. J., and Firestone, J.: Improving Spatial Representation of Global Ship Emissions Inventories, Environ. Sci. Technol., 42, 193–199, doi:10.1021/es0700799, 2008.

Wang, Z. L., Zhang, H., and Zhang, X. Y.: Simultaneous reductions in emissions of black carbon and co-emitted species will weaken the aerosol net cooling effect, Atmos. Chem. Phys., 15, 3671–3685, doi:10.5194/acp-15-3671-2015, 2015.

Wild, M.: Global dimming and brightening: A review, J. Geophys. Res.-Atmos., 114, D00D16, doi:10.1029/2008JD011470, 2009.

Yu, H., Kaufman, Y. J., Chin, M., Feingold, G., Remer, L. A., Anderson, T. L., Balkanski, Y., Bellouin, N., Boucher, O., Christopher, S., DeCola, P., Kahn, R., Koch, D., Loeb, N., Reddy, M. S., Schulz, M., Takemura, T., and Zhou, M.: A review of measurement-based assessments of the aerosol direct radiative effect and forcing, Atmos. Chem. Phys., 6, 613–666, doi:10.5194/acp-6-613-2006, 2006.

Zhang, K., O'Donnell, D., Kazil, J., Stier, P., Kinne, S., Lohmann, U., Ferrachat, S., Croft, B., Quaas, J., Wan, H., Rast, S., and Feichter, J.: The global aerosol-climate model ECHAM-HAM, version 2: sensitivity to improvements in process representations, Atmos. Chem. Phys., 12, 8911–8949, doi:10.5194/acp-12-8911-2012, 2012.

Zhao, T. X.-P., Yu, H., Laszlo, I., Chin, M., and Conant, W. C.: Derivation of component aerosol direct radiative forcing at the top of atmosphere for clear-sky oceans, J. Quant. Spectrosc. Ra., 109, 1162–1186, doi:10.1016/j.jqsrt.2007.10.006, 2008.